TRANS-SONICS

CAPACITANCE PROPELLANT GAGING STUDY FOR ORBITING SPACECRAFT

FINAL DEVELOPMENT REPORT

JUNE 1967

Prepared for:

National Aeronautics and Space Administration

George C. Marshall Space Flight Center

Huntsville, Alabama 35812

TRANS-SONICS, INC., BURLINGTON, MASSACHUSETTS

TRANS-SONICS, INC., BURLINGTON, MASSACHUSETTS
tel. 272-1000—*area code:* 617-TWX: 710-332-1635—TELEX 094-6295 *please reply to* P. O. BOX 326, LEXINGTON, MASS. 02173

CAPACITANCE PROPELLANT GAGING STUDY FOR ORBITING SPACECRAFT

FINAL DEVELOPMENT REPORT

JUNE 1967

Prepared for:

National Aeronautics and Space Administration

George C. Marshall Space Flight Center

Huntsville, Alabama 35812

TABLE OF CONTENTS

ILLUSTRATIONS

ABSTRACT

A unique approach to the problem of gaging propellant tanks in a zero gravity environment has been investigated. A capacitance technique is used in which surface electrodes are attached to the inside tank wall so that the whole tank becomes the inside of a capacitor. The shapes and potentials of the electrodes are adjusted so that the interior electric field is approximately uniform throughout the tank, insuring equal weighting to all regions, regardless of how the liquid is distributed.

A theoretical analysis of the field distribution in a cylindrical tank was conducted. This showed that satisfactory uniformity can be obtained with a reasonable number of electrodes. It also showed that the errors caused by the surface charges on the liquid interfaces are not significant in the cases of liquid hydrogen and liquid oxygen, particularly if the readings are averaged over two orthogonal directions of the field.

An experimental investigation was conducted in which a cylindrical tank with one hemispherical end was constructed, and sixteen (16) electrode strips were installed. A breadboard electronic system was built and tested with the model tank. The results were satisfactory, except that the method for eliminating the "leakage" capacitance to the tank wall was found to be inadequate. New methods for overcoming this problem were evolved, but not tested.

INTRODUCTION

With the current interest in manned space missions, a number of new technical problems have arisen which must be solved in order to insure the safety of these missions.

One such problem is the accurate gaging of liquid propellants in orbiting vehicles, where gravity is essentially absent. Since fluid behavior becomes wholly different in zero-gravity, due to the dominance of capillary forces, the conventional techniques for propellant gaging are obsolete. Hence, new schemes are needed to solve this problem.

In the gaging of liquid propellants, there are a number of possible approaches. Each approach falls into one of two categories, depending on whether the propellant mass is inferred from measurements made on the vapor ullage or whether the propellant mass is measured directly.

The ullage techniques have the advantage of being less dependent on the geometry of the tank or the orientation of the propellant than are the direct mass measuring schemes. The truth of this lies in the fact that they are concerned with the measurement of one or more of the thermodynamic parameters which are independent of geometry, rather than relying on the measurement of some material property (absorption coefficient, dielectric constant, etc.) which requires geometry-dependent arrays of sources and detectors. However, the ullage schemes are not advantageous insofar as the very thermodynamic parameters upon which the measurement depends, in most cases, cannot be adequately controlled to be properly measured because of changing thermal inputs, venting requirements in some cases, response times, vapor condensation and, in general, the persistent presence of thermodynamic transients. Although conditions of thermodynamic equilibrium are not necessary in the mass schemes, a major drawback is that they are geometry-dependent and require statistical averaging techniques to eliminate the resulting errors.

Under this contract, a study has been made to determine the feasibility of using a mass measuring scheme based on capacitance for solving the zero-g gaging problem. The use of capacitance techniques for the measurement of liquid level and fluid quantity in one-g is well established. The proportionality of average mass density ρ to dielectric constant ϵ expressed by the Clausius-Mosotti relation:

$$\rho = K \frac{\epsilon - 1}{\epsilon + 2}$$

makes this technique applicable.

Under the influence of gravity, and in containers of known volume, the measurement of the effective dielectric constant of liquids of known density can be calibrated accurately to read fluid level directly. Similarly, in zero-g and in tanks of known volume, a measurement of the effective dielectric constant of a two-phase (liquid/vapor) fluid gives a measure of the average density and, therefore, the total liquid mass. However, in zero-g, where surface tension forces predominate, the configurations of confined two-phase fluids are variable and unpredictable. Because these configurations lack the usual flat liquid/vapor boundary which occurs under the influence of gravity, the conventional point level or continuous level gages are not adequate. Furthermore, the presence of a sensing device within the tank enclosure could affect the propellant distribution because of the capillary forces; i.e., probes of the usual tubular or coaxial design would tend to draw up and contain the propellant, thereby indicating the presence of a greater mass of propellant than actually exists.

In view of these considerations, a completely new capacitance gaging concept is necessary. In the determination of a new capacitance design, it is necessary to meet some unusual requirements. The most fundamental of these requirements is that the gage must perform in a manner which does not allow any region of the tank volume to be weighted more heavily than any other. This

requirement arises because in zero-g practically every region (aside from those regions near internal structures) is equally likely to contain fluid. Previous attempts to meet this requirement have resulted in gage designs comprised of a matrix of wire electrodes distributed throughout the tank volume, dividing the space into small cells, each monitored independently and then averaged. Although this approach seems capable of attaining the desired measurement, it is heavy and cumbersome to fabricate.

Just prior to this contract, however, a capacitance technique was devised which circumvents the aforementioned difficulties very well. In the present concept, it is not necessary to physically partition the tank space into cells in order to monitor each region equivalently. Equal weighting of the tank space can be accomplished by establishing a suitable electric field configuration within the tank space using electrodes mounted only on the tank walls. Furthermore, by properly designing these electrodes, their influence on positioning the fluid can be made negligible.

This new concept attempts to solve the zero-g gaging problem, not by incorporating separate probes, but by utilizing the basic tank as a "level" gage, whereby the judicious choice of electrodes on the tank walls allows the accurate measurement of propellant quantity in the tank almost independent of its configuration.

Background Information: Before discussing the gage concept and the results of the feasibility study, it is advantageous, for the purposes of reference, to give a brief discussion of the actual SIV-B tank, its internal structures, and the physical properties of the propellants LH_2 and LOX which are of relevance in this contract work.

The SIV-B Tank: The SIV-B, built by Douglas Aircraft Company, is the upper stage of both the Saturn 1B and Saturn V rockets.

The stage is essentially cylindrical and is 58.4 feet long by 21.7 feet in diameter. The propellant tank is 21.7 feet in diameter and 44 feet long. It features two dome-type ends and an intermediate insulated bulkhead separating the liquid hydrogen tank from the oxygen tank. The tanks are made of aluminum alloy with the inner surfaces milled in a waffle-like pattern. In the hydrogen tank, for purposes of thermal insulation, each recessed "square" is filled with a polyurethane and fiber glass block and, when all squares are filled, smooth coated with a polyurethane and fiber glass layer. This insulation is about an inch thick. Figure 1 illustrates the configuration of the stage and its propellant tanks.

The hydrogen tank contains a number of internal components and structures. These include slosh baffles, pressure bottles, instrumentation probes as well as the previously-mentioned insulating layer.

There are two annular slosh baffles in the LH_2 tank. They are made of nylon mesh and are anchored to the inner surface of the tank. Each of these nylon baffles is about three feet wide and are interwoven with nylon rope for support. The first of these is located about ten feet below the tank top and the second is further down. There are eight helium pressure bottles attached to the inner wall of the tank. They are each spherical with a diameter of about two feet. There are also two instrumentation probes which run over most of the tank length. These probes hold the sensors for the propellant utilization system, temperature measurements, etc.

The LOX tank has a single centralized instrumentation probe and some structural supports and ducting. It does not have the fiber glass insulation found in the LH_2 tank.

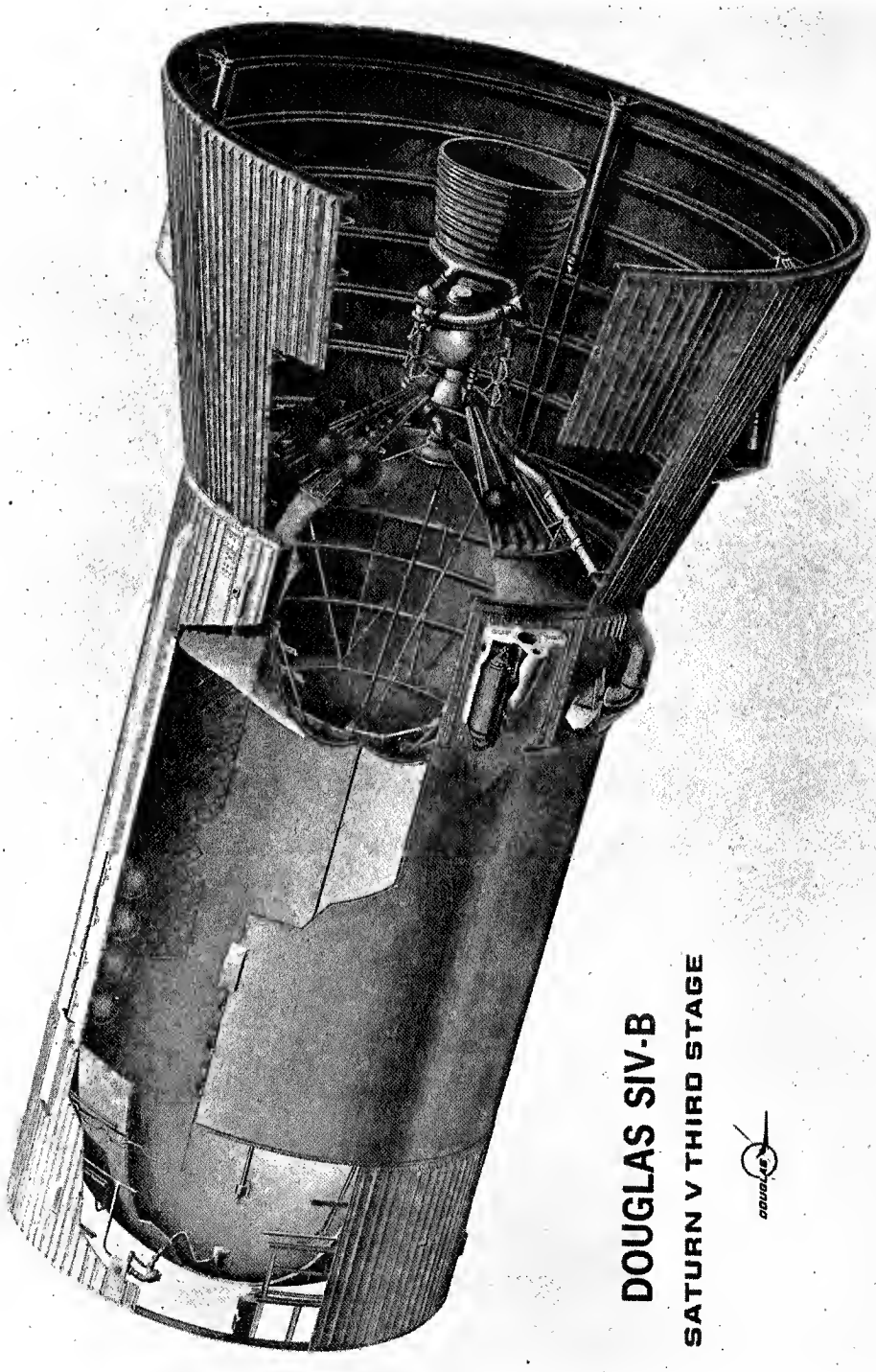

Figure 1

Propellant Properties: The propellants considered in this feasibility study are the cryogenic fluids LOX and LH_2. The ratio of density to surface tension for these propellants at their boiling point temperatures is of the order of a few hundredths of a $gm/cm^2/dyne$, which means that even in acceleration fields as low as 20 micro-g's, their hydrostatic behavior will begin to be gravity dominated (Bond number$\approx$1) in tanks as large as the SIV-B. This indicates that in low orbit missions, where aerodynamic drag may be of this order, the liquid/vapor configuration will approach that in which the vapor is maintained "above" the liquid. In a more nearly ideal zero-g environment, the liquid/vapor configuration can take a number of forms. However, surface tension, thermal gradients, and the almost totally wetting character of these cryogens will tend to cause engulfed ullage to migrate along thermal gradients toward the warmest portion of the tank wall. Because of the zero contact angle of these propellants, the ullage will form nearly spherical interfaces with the liquid.

However, these simple and completely static configurations will be constantly perturbed by external accelerations caused by attitude control, venting, etc., and by propellant boiling and cavitation. For these reasons, the chosen gaging scheme and the experimental portion of the feasibility study does not rely heavily on these configurations but attempts to evaluate the system under more general considerations.

The electrical properties of LH_2 and LOX are highly appropriate for the present gaging technique. These propellants have extremely high electrical resistance so that their electrical response is completely reactive, which is required. Also the dielectric constants are small enough so that errors introduced by dielectric shielding are not large, yet these constants are big enough to allow a substantial change in gage impedance between empty and full tank. The relative dielectric constant of LH_2 is about 1.23 and that of LOX approximately 1.5.

PROGRAM PURPOSE

This report describes the work that has been performed under NASA Contract NAS8-18059. The total contract period covered is from July 25, 1966, to January 15, 1967.

Contract Objective: The objective of the contract has been to perform a feasibility study of capacitance techniques for mass gaging of propellants in zero-g. In particular, the chosen technique was to be capable of performing to all requirements listed below when used in the main LOX and LH_2 tanks of the Saturn SIV-B stage, as well as in small tanks on the order of 8' x 4'. Emphasis was to be placed on proving feasibility for the SIV-B stage, since it was assumed that this was enough to insure feasibility for smaller tanks.

The basic performance requirements of the gaging system were set forth as follows:

> The propellant measuring system shall measure the total mass of propellant (liquid hydrogen or LOX) in the tanks to an accuracy of ±2% of full scale or better.
>
> This accuracy shall be achieved only when the propellant is essentially in static equilibrium such that the vapor ullage is confined to a single "bubble" located somewhere in the tank.
>
> This accuracy shall be achieved in acceleration environments of zero-g to five g's. However, if special considerations are necessary to achieve this accuracy in higher g's, emphasis shall be placed on meeting this requirement in zero-g.
>
> The response time of the propellant gaging system shall be 0.5 seconds or less.

To meet these requirements, a new capacitance scheme was devised and evaluated under this contract.

The tank was to be designed in all essential details including mock-ups of internal structures (slosh baffles, helium bottles, probes, etc.). Furthermore, scaling laws for the model were to be established so that a valid prediction of the performance of a full-scale gage could be made from the test data for the model.

For the purposes of evaluating the experimental performance of the model gage, a zero-gravity environment was to be simulated by using either two equidensity, immiscible fluids with different dielectric constants or by simulating zero-g fluid configurations by appropriately molded materials of low dielectric constants (such as polyurethane foam).

I. GAGING SYSTEM CONCEPT

The capacitance concept studied under this contract is designed to meet certain physical requirements which are necessary to insure the development of an accurate zero-g propellant gaging system. The underlying effort in the approach is to devise a design which takes full advantage of the tank geometry in the generation of the sensing field so that unnecessary electrode structures within the tank space are avoided.

For this reason, the concept utilizes the tank walls as a desirable location for the placement of the source and sensing electrodes. The specific physical design of these electrodes and the potentials applied to them are determined by both the tank shape and the desired field configuration within the tank space.

1.1 Ideal Field Configuration: In a zero-g application, it is necessary to generate a field which samples each point of the tank space equivalently so that liquid in one region is not weighted more heavily by the measurement than an equal amount of liquid elsewhere. Since the weighting is proportional to the field strength at each point, this is accomplished best by a field configuration which is uniform; i.e., identical to the field of a parallel plate capacitor.

To generate a uniform field in a tank which has curved boundaries, it is required that a distribution of source potentials be impressed on these boundaries. In fact, to generate a perfectly uniform field inside of a tank with curved walls, this potential distribution must be a continuous function of the coordinates specifying the wall geometry. To be more specific, in Appendix A we have calculated the required boundary potential functions for a cylinder and a sphere when the uniform field is established transverse to the tank axis.*

*It is also possible to choose the direction of the field parallel to the tank axis; however, this is unattractive for the following reasons: First, the electric field must be parallel to the cylindrical portion of the tank and this would require a considerable number of electrodes (circular bands) to maintain. Second, the boundary potential must be a linear function along the tank length. This would mean that none of the individual potentials would be the same, as in the present case, so that considerably more transformer taps would be necessary.

For example, at the cylindrical wall of the LH_2 tank, the circumferential variation of potential must follow the relation:

$$V(\theta) = V_o \cos\theta \qquad (1.1)$$

while for both the hemispherical domes of the LH_2 tank and the entire LOX tank (assumed spherical) the potential must obey:

$$V(\theta, \phi) = V_o \sin\phi \cos\theta \qquad (1.2)$$

The value V_o is determined by the product of the desired electric field E and the tank radius R, and these expressions are the correct forms which match E and V along the dome-cylinder junctions.

As a consequence of the required variations of potential along the cylindrical or spherical tank boundaries, it is not possible to have a single conductor, like the tank wall, possess this boundary potential. For a real gage, the ideal case can be approximated only by incorporating within the tank an array of separate conductors which conform to the geometry of the walls and which carry potentials in accordance with the relations (1.1) or (1.2), depending on the angular coordinate(s) of the conductor position. For example, on the cylindrical wall, a number of conductor strips of prescribed width extending the length of the wall can be bonded to the wall insulation (or fastened close to the wall by other means) so that each strip is parallel to its neighbor and separated from it by a small distance. To each strip the correct potential is applied using (1.1). Obviously, the more strips that are included, the more exact is the approximation to the ideal case. However, if a very large number of strips were required, it would not be a very attractive scheme for mass gaging. It turns out, as we have theoretically and experimentally verified and discuss in Section III, that a large number of electrodes is not required and that fewer than twenty electrodes produces a field of considerable uniformity.

Applying the same technique to the spherical LOX tank or the hemispherical end caps of the LH_2 tank, the problem is more complex because of the required potential variation in the two angular directions, θ and ϕ. Here, use can be made of a number of "patch sensors" which are excited with potentials in accordance with Equation (1.2).

Because of the necessity of using a discrete array of boundary electrodes in a real gage, it is not possible to generate a perfectly uniform field. For this reason, one of the important tasks in the feasibility study is the determination of the number, widths, spacings, and angular positions of the conductors in the array to produce a field of optimum uniformity for the application. We present the electrode design analysis in Section III.

1.2 Averaging Concept: There is a second physical requirement which the gage concept may have to be capable of meeting. This requirement has to do with the dependence of the gage capacitance on propellant orientation. Even though the use of a uniform field guarantees that equal fluid elements at any point in the tank space will contribute equivalently to the gage capacitance, strictly speaking, this is only true if the fluid elements have the same shape and orientation. This effect arises as the result of the induced surface charges which the field creates at dielectric interfaces. The magnitude of these charges depends on the direction of the field relative to the boundary. Fluid elements with surfaces parallel to the flux lines add directly to the dielectric value (parallel capacitance case) while elements with boundaries normal to the field lines always contribute less (series case). The effect is known as dielectric self-shielding and is greatest for materials of high dielectric constant. In the present application, the fluids LH_2 and LOX have fairly low dielectric constants so that errors introduced by shielding will be correspondingly small. However, it is possible to reduce these errors by an averaging

technique which involves applying two orthogonal fields on a time sharing basis, or by completely rotating the field about the tank axis and averaging the individual measurements. It is not clear at this point whether averaging is really necessary with LH_2 or LOX since their dielectric constants are small. Furthermore, if the supposed spherical ullage bubble configuration is actually valid in zero-g, the averaging scheme would not be effective anyway, because of the bubbles' symmetry. For these reasons, and because the inclusion of this technique would complicate the electronics considerably, the experimental portion of the present program did not include averaging. Instead, stress was placed on evaluating the basic physical and electronics concepts to determine if a simpler design could achieve the desired characteristics. The need for averaging would then depend on whether or not the simpler concept could be made adequate.

1.3 Measurement Concept: The final requirement which the gage concept must meet is that the measurement technique must result in an output signal which is proportional only to the quantity of propellant in the tank. Furthermore, this signal must be large enough so that the minimum signal resolvable by the measuring circuit is well below it and within the desired accuracies.

The measurement problem is illustrated by the simplified circuit shown in Figure I-1. The problem is to measure the capacitance C, which is a function of the propellant quantity, while maintaining electrodes 1 and 2 at potentials $+V$ and $-V$ respectively. These potentials are necessary in order to provide the approximately uniform field so that the measurement will be relatively independent of the propellant distribution in the tank as described in an earlier section of this proposal.

The measurement must be made by a scheme in which the result is not affected by variations in C_1 and C_2 which are large compared to C. C_1 and C_2 consist of capacitances from the electrodes to the tank wall and cable capacitances. C_1 and C_2 are of the order of 1000 times the full-scale value of C.

Finally, the measurement scheme should "subtract out" the empty-tank value of C. The capacitance C may be written:

$$C \cong C_o \left[1 + (\epsilon - 1) \frac{m}{M} \right] \tag{1.3}$$

where C_o is the value of C when the tank is empty

ϵ is the relative dielectric constant of the liquid propellant
m is the mass of liquid propellant
M is the capacity of the tank in terms of liquid propellant mass.

The quantity to be measured is the second term; i.e.,

$$\Delta C = C - C_o \cong (\epsilon - 1) \frac{m}{M} C_o \tag{1.4}$$

which is a measure of the propellant mass.

The circuit of Figure I-2 performs the desired measurement. The operation of this circuit may be described more simply by the use of an equivalent circuit referred to the primary side of T_1. This circuit is presented in Figure I-3. The system is excited by an oscillator which provides the potentials V and -V, which are alternating at a low RF rate, for example, 100 KHz. With the switches in the position shown,

$$I_1 = V \left(jwC_1 + jwC_2 + jw4C - jw4C'_o + \frac{1}{jwL_1} \right)$$

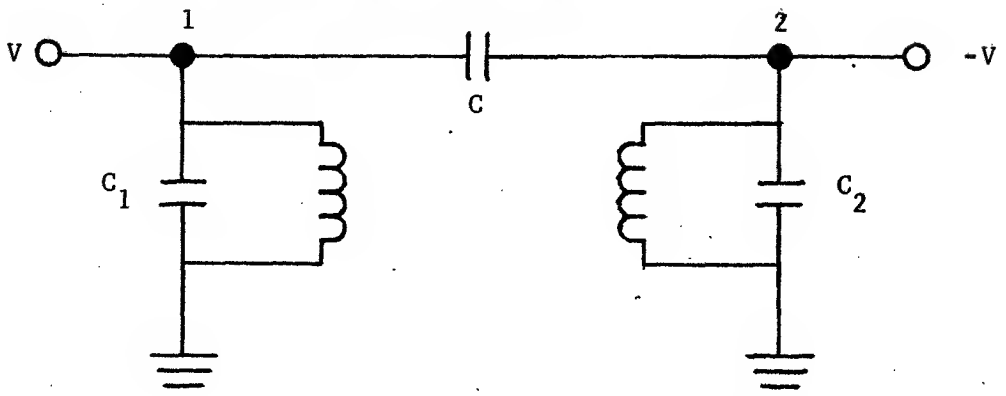

Simplified Representation of Circuit

Figure I-1

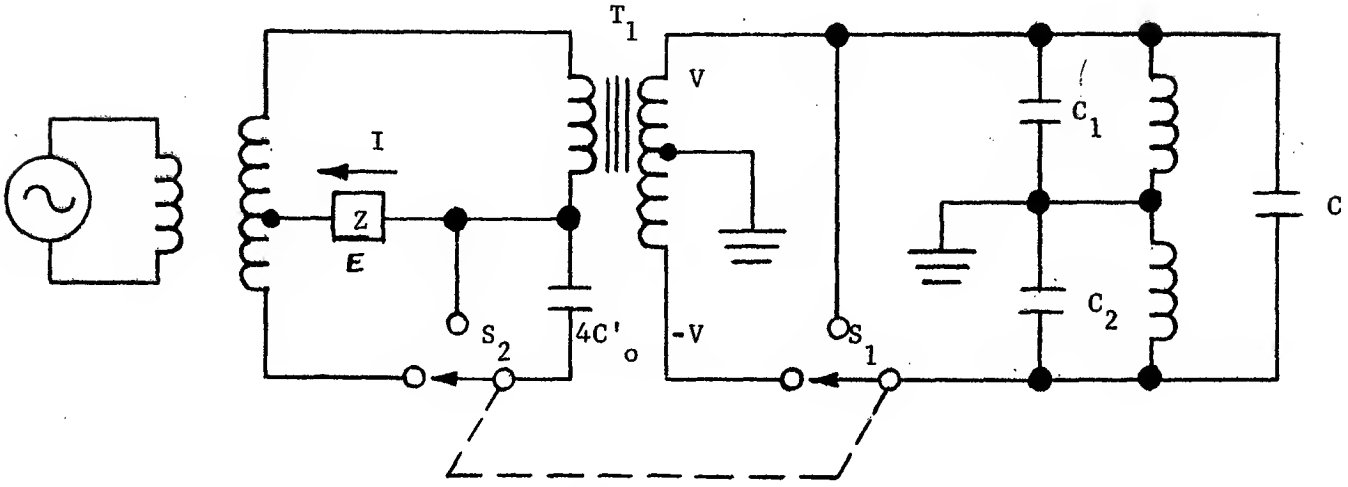

Simplified Measuring Circuit

Figure I-2

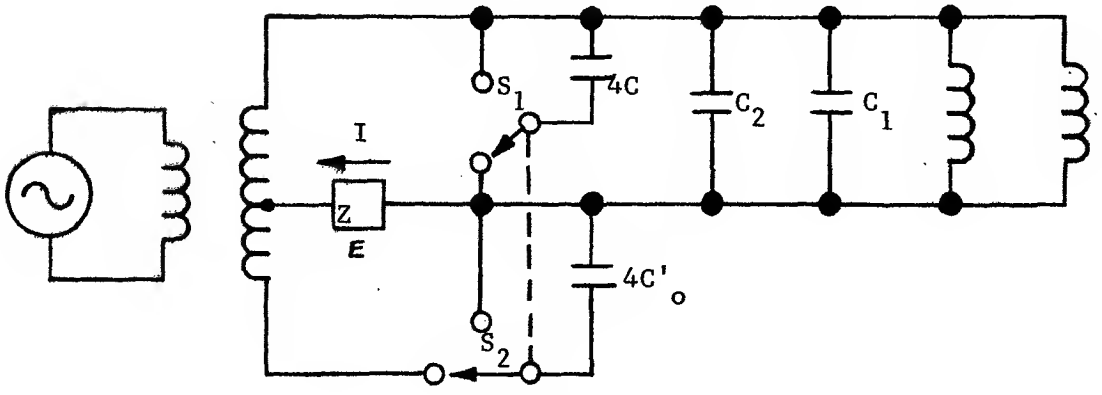

Equivalent Circuit

Figure I-3

and with the switches in the alternate position,

$$I_2 = V(jwC_1 + jwC_2 + \frac{1}{jwL_1})$$

The difference between these is,

$$I_1 - I_2 = V \left[jw\ (4C - 4C'_o) \right] \qquad (1.5)$$

If C'_o is adjusted to be equal to C_o, the empty-tank value of C, then $I_1 - I_2$ is proportional to the ΔC of equation (1.4).

The current I is, therefore, a square-wave-modulated signal in which the peak-to-peak value of the modulation is proportional to the propellant quantity. Although the "carrier" current is a function of C_1, C_2, and L_1, which are large quantities and may not be stable, the modulation is independent of all of these quantities.

In order to have an accurate measurement it is necessary that V and ω, the amplitude and frequency of the source, be stable to somewhat better than the measurement accuracy, and also that the amplifiers and detectors operating on E be similarly stable. Stabilities on the order of 1/4% are required; such stabilities are readily achieved in reliable space-tested hardware.

In the actual measuring system, the transformer T_1 has a secondary with multiple taps in order to provide the proper potentials to the various electrodes. Figure I-4 shows the system for a twelve-electrode configuration, for one of two spatially orthogonal fields. With the transformer winding as shown, the capacitance C_o is approximately

$$C_o = \frac{\pi}{4} \epsilon \mathcal{L}$$

where ϵ is the absolute dielectric constant in farads per meter and ℓ is the length of the tank in meters. For a tank of 10 to 15 feet long, C_o is approximately 30 picofarads. Of course, by altering the turns-ratio of the transformer, this capacitance (referred to the primary) may be made any convenient value. To make the system less sensitive to propellant distribution, two spatially orthogonal fields are used on a time-shared basis, and the outputs are averaged. The two systems utilize the same set of electrodes within the tank. Semiconductor switches operated at a low frequency (e.g., 500 Hz) alternately connect the electrodes to the potentials as shown in Figure I-4 and in a similar configuration rotated 90^o in space.

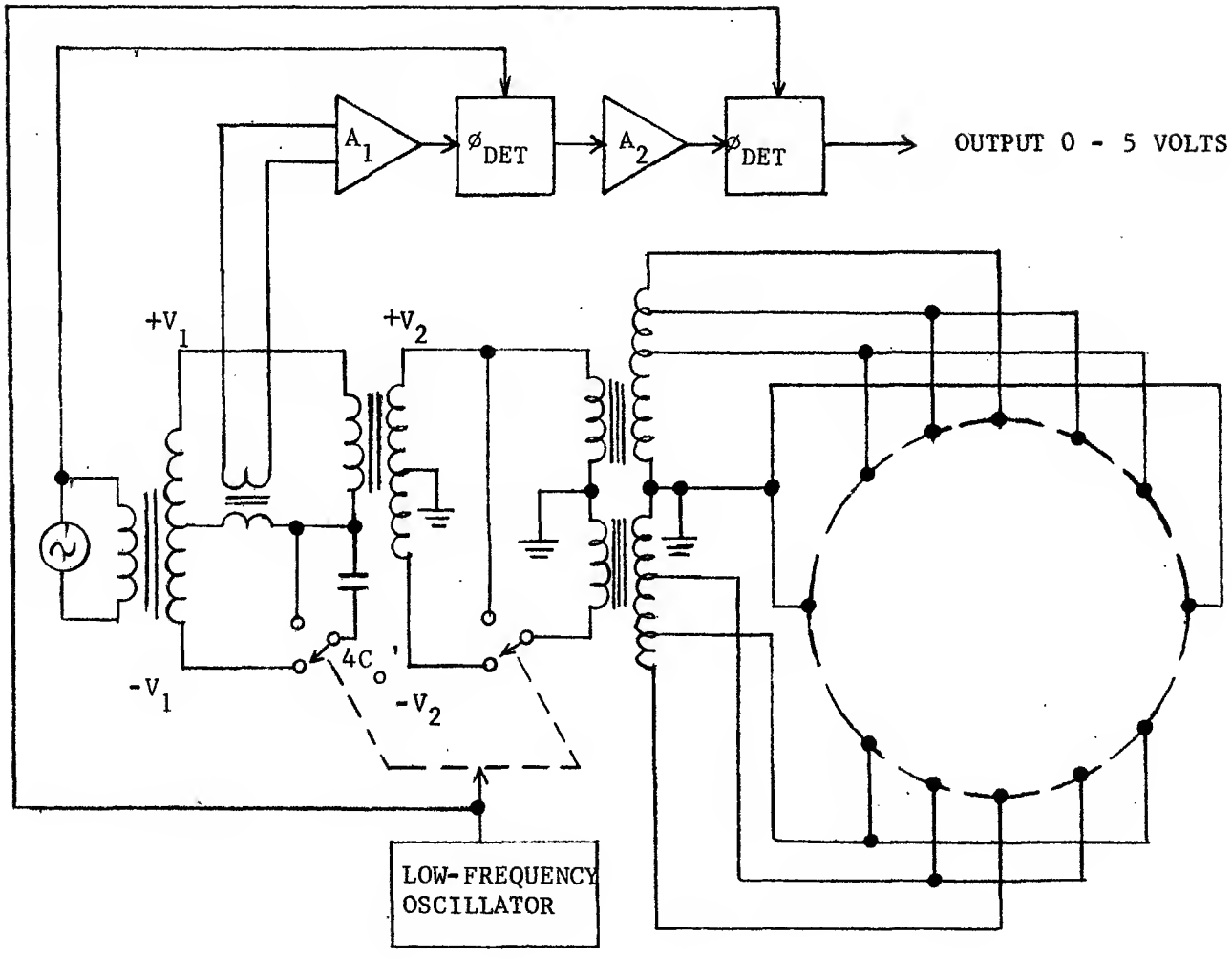

Capacitance Mass Gaging System

Figure I-4

II. PERFORMANCE ANALYSIS OF AN IDEAL GAGE

As a preliminary to the theoretical analysis of the actual gage, we present here a performance analysis of an ideal gage in order to demonstrate the basic soundness of the uniform field concept. The approach here is completely analogous to that used in a later section where the analysis of the actual gage is presented. However, the mathematical treatment in this case is much simpler and as a result, more lucid.

We will perform two basic calculations. The first will be a calculation of the approximate empty tank capacitance of the gage to show that this concept is capable of meeting the requirements of the measuring circuit; i.e., the minimum capacitance criterion. The second calculation will treat gage performance when propellant is included in the tank to determine whether or not the concept can perform with the desired ±2% accuracy.

The assumptions which are made in this analysis are the following: First, the gage is assumed to be ideal. This simply means that it represents the ideal limit of the actual gage so that a continuous $\cos\theta$ potential can be established on the tank boundary. This implies a gage with infinitely many boundary electrodes, each electrode strip of infinitesimal width. Second, the hemispherical endcaps of the tank are neglected and the tank is viewed as a cylinder of infinite length. This allows a simpler solution of LaPlace's equation. The capacitance calculated from this model is, therefore, one per unit of tank length. Third, in the performance calculation, the error is computed as a percent (of full tank) deviation from the ideal linear response.

2.1 Tank Capacitance: Aside from the errors introduced by stray capacitances, propellant orientation, etc., there will also be some intrinsic error associated with the measuring circuit. This error will place a limit on the resolving power of the circuit for measuring the gage impedance. This, in turn, will require that the gage possess some minimum (empty tank) capacity in order that this intrinsic error is well within the desired gage accuracy.

If we designate the empty-tank capacitance of the gage as C_o, then the change in gage capacitance from empty to full tank is given by,

$$\Delta C = (\epsilon / \epsilon_o - 1) \, C_o \tag{2.1}$$

where ϵ / ϵ_o is the relative dielectric constant of the propellant. Now, if the limit of resolution of the measuring circuit is δC, then this will correspond to some intrinsic volume error ΔV in measuring propellant quantity, expressed by:

$$\Delta V = \frac{\delta C}{\Delta C} \, V_o \tag{2.2}$$

where V_o is the total tank volume. Therefore, since it is desired to keep ΔV small compared to errors contributed from other sources, a condition is implied on C_o; i.e.,

$$C_o \geq \frac{1}{(\frac{\epsilon}{\epsilon_o} - 1)} \quad \frac{V_o}{\Delta V} \, \delta C \tag{2.3}$$

Presently, Trans-Sonics is producing quantity gaging circuits capable of resolving capacitance changes of the order of 7×10^{-3} picofarads. Using this value, assuming LH_2 is the propellant (worst case $\epsilon / \epsilon_o = 1.23$) and requiring that the intrinsic quantity error $\Delta V / V_o$ should not be greater than 0.1%, the minimum empty tank capacitance must be

$$C_o \approx 30 \text{ pf}$$

The present gage concept is capable of meeting this requirement. In the next section, the expression for the cylindrical tank capacitance is derived and, rewritten here, is

$$C_o = \frac{\pi}{4} \quad \epsilon_o L, \tag{2.4}$$

where L is the tank length in meters and $\epsilon_o \cong 8.85 \times 10^{-12}$ f/m (vacuum value). This gives a total empty tank capacitance in the vicinity of 50 picofarads or more for the S-IVB tank.

Since the change in capacitance from full tank to empty tank for LH_2 will be about 20% of this, or 10pf, it is expected that mass changes of the order of a 0.1% of full scale will be resolvable. Thus, it is clear that no difficulties arise with respect to signal to noise when resolving mass quantity to within one or two percent.

2.2 Performance Analysis: A derivation of the error signal as a function of dielectric constant and propellant quantity is given below and is calculated for the case in which the propellant/vapor interface is a cylindrical surface concentric with the tank wall. The fuel is contained in the region between this interface and the wall. See Figure (II-1). This configuration can be considered as a gross idealization of the zero-g situation in which the propellant is capillary dominated and completely wets the wall, engulfing its ullage. In a real situation, the ullage bubble would migrate to the wall, usually to a warmest point. However, for our purposes we can obtain from this case an idea of the error due to fluid configuration. Furthermore, it is an interesting case in that its circular symmetry does not make it amenable to any type of field averaging (as would be the case with a spherical bubble in an actual tank); and, therefore, the errors are irreducible except by calibration.

Consider a cylindrical tank of radius R with its center at the origin of a cylindrical coordinate system. Assume the potential

$$V(R) = V_o \cos\Theta \qquad (2.5)$$

as the given boundary condition. Now assume that the boundary between a liquid of dielectric constant ϵ_2 on the tank walls and a gas of dielectric constant ϵ_1 in the center of the tank is a cylinder of radius a, coaxial with the tank.

The solution of Laplace's equation gives the expression for the potential in the gas as

$$V_1 = A r \cos\theta \tag{2.6}$$

and that in the liquid as

$$V_2 = (Br + c/r)\cos\theta \tag{2.7}$$

where A, B, and C are constants to be determined by considering the field conditions at the dielectric boundary at r = a. These conditions are

$$\epsilon_1 \frac{\partial V_1}{\partial r} = \epsilon_2 \frac{\partial V_2}{\partial r}$$

and

$$V_1(a) = V_2(a) \tag{2.8}$$

That is,

$$\epsilon_1 A \cos\theta = \epsilon_2 (B - C/a^2)\cos\theta \tag{2.9}$$

and

$$Aa = Ba + C/a \tag{2.10}$$

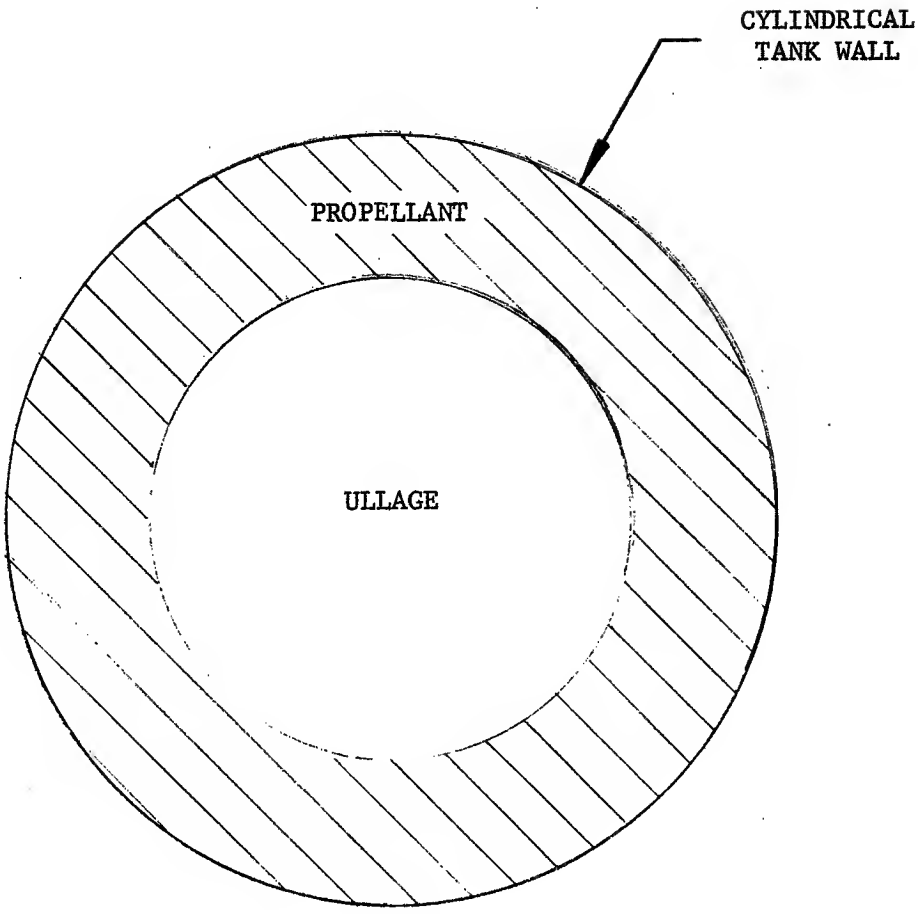

Figure II-1
IDEALIZED PROPELLANT CONFIGURATION

At r = R we have, from (2.5) and (2.7),

$$BR + C/R = V_o \tag{2.11}$$

Solving (2.9), (2.10), and (2.11) yields

$$A = \frac{V_o}{R} \frac{1+\beta}{1+p^2\beta}$$

$$B = \frac{V_o}{R} \frac{1}{1+p^2\beta}$$

$$C = \frac{V_o}{R} \frac{2}{1+p^2\beta}$$

where

$$\beta = \frac{\epsilon_2 - \epsilon_1}{\epsilon_2 + \epsilon_1}$$

and

$$p = a/R$$

A capacitance per unit length may be defined as the charge on one half of the cylinder, per meter of length, divided by the potential $2V_o$; thus

$$C = \frac{1}{2V_o} \int_{-\frac{\pi}{2}}^{\frac{\pi}{2}} R\epsilon_2 (B - C/R^2) \cos\theta \, d\theta$$

or

$$C = \frac{\pi}{4} \epsilon_2 \left[\frac{1 - p^2\beta}{1 + p^2\beta} \right] \tag{2.12}$$

If C_o is the capacitance of the empty tank; i.e., for a = R, then $C_o = \frac{\pi}{4} \epsilon_1$ and

$$C - C_o = \Delta C = \frac{\pi}{4} \left[(\epsilon_2 - \epsilon_1) - \epsilon_2 \frac{2p^2\beta}{1+p^2\beta} \right] \qquad (2.13)$$

Now, if $(1 - p^2) = v$ = normalized liquid volume, (that is, v = liquid volume divided by total tank volume), then we would like to have

$$\Delta C_{ideal} = \frac{\pi}{4} v (\epsilon_2 - \epsilon_1). \qquad (2.14)$$

$$\frac{\Delta C - \Delta C}{\Delta C_{max}}_{ideal} = \frac{v(1-v)}{\frac{1}{\beta}+(1-v)} \qquad (2.15)$$

The results of this calculation are summarized in Figures II-2 and II-3. In both figures, δC is the capacitance deviation from linearity and ΔC is the total change in gage capacitance from full to empty tank. In Figure II-2 the fractional $\delta C/\Delta C$ error is given as a function of the fraction of propellant in the tank. Figure II-3 displays the maximum error (maximum points of Figure II-2) as a function of relative dielectric constant of the fuel. Just for reasons of comparison, the error bands for several fuels have been computed. It is interesting to note from (2.15) that even in the case of $\epsilon \to \infty$ (See Figure II-3) the worst deviation is about 17%. For the fuels of interest, hydrogen and oxygen, the maximum uncalibrated errors are about 2% and 4% respectively and this occurs only when the tank is about half full. Calibrated, these errors become ±1% and ±2% respectively. Since these errors are based on an unlikely fluid configuration as well as a condition which does not involve averaging, it appears clear that the gage concept proves quite feasible for measuring propellant mass to within the desired accuracies.

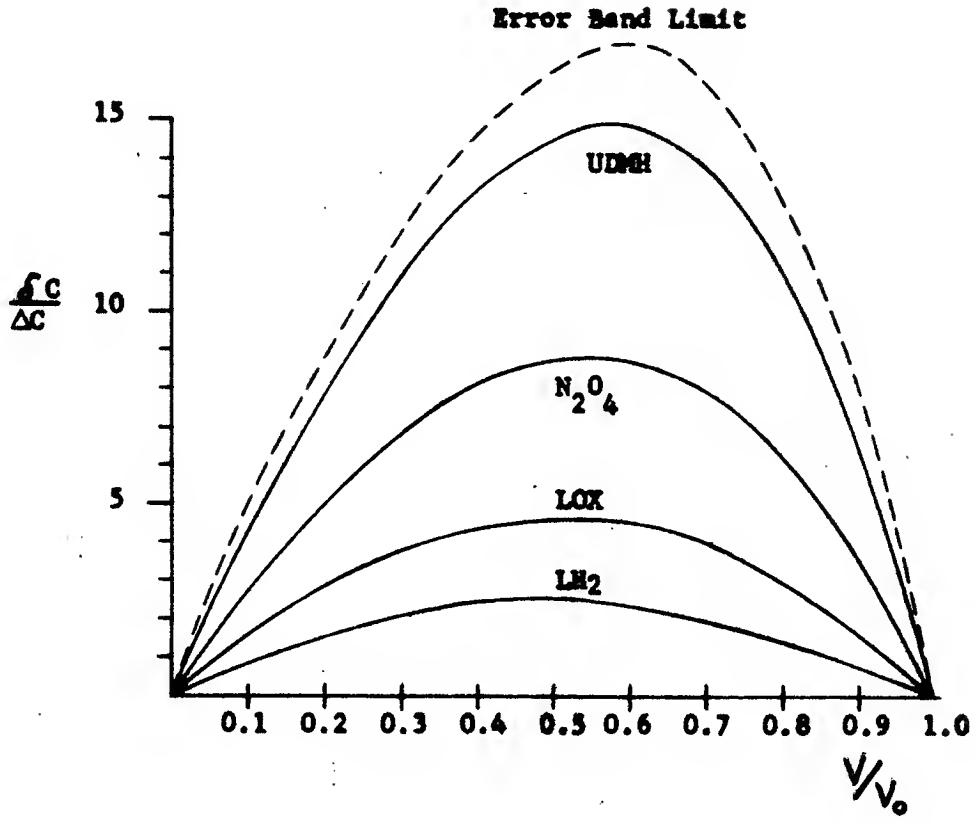

Figure II-2

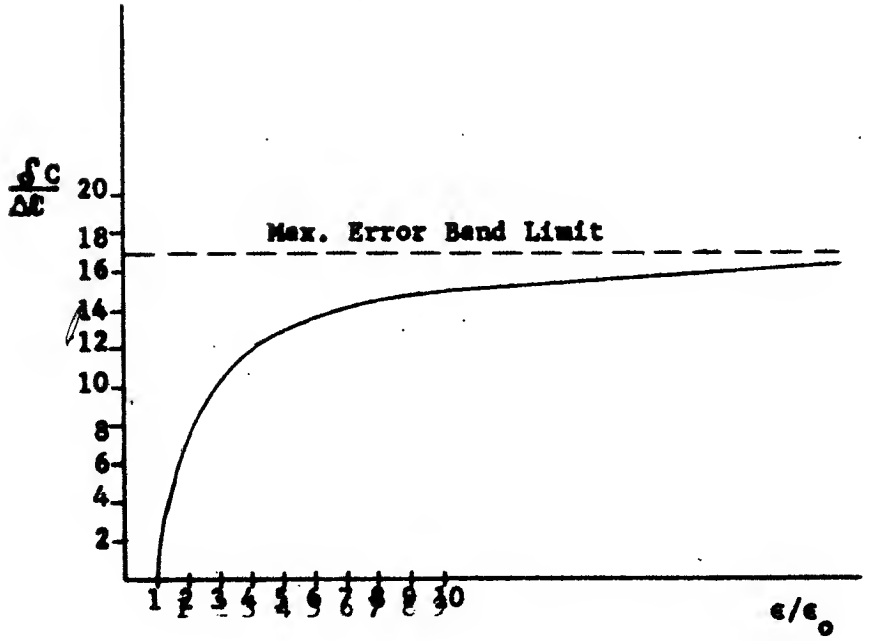

Figure II-3

III. GAGING SYSTEM DESIGN

The design of the actual gaging system is concerned primarily with two areas. These include the design of the electrode configuration and the design of the measuring circuit. The ultimate design of the measuring circuit depends, for the major part, on the resultant electrode configuration. For this reason, we will consider the circuit design last.

The design of the electrode configuration is of utmost importance in determining the ultimate achievable accuracy of the scheme. For example, in the previous section we demonstrated that the desired accuracies could be achieved if a perfectly uniform field is generated within the tank. However, even with the ideal gage configuration, the achievable accuracies (at least for the propellant configuration analyzed) do not leave a large margin for additional errors. For this reason, the ability to generate a highly uniform field by a finite set of discrete electrodes on the tank boundary is crucial to the success of the concept. Thus, in order to ascertain concept feasibility, the electrode design study is necessarily comprehensive; and is, therefore, a major task of the program.

The analysis performed during this contract, in determining the optimum electrode design, is extremely involved mathematically and contains a considerable volume of tedious calculations, both formal and numerical. To avoid cluttering the main issues of the analysis, the primary attempt in this section will be to present the fundamental theory underlying the mathematical approach. As will become evident, much of the initial computational effort is now less important since the conclusions drawn from it are sufficiently simple, in retrospect, that some of these

calculations seem superfluous. However, at the time, this was not so because the conclusions drawn could not be known a priori, and it was only after these calculations were performed that the picture became adequately clear.

Thus, for the purposes of this report, only the main conclusions will be presented here. However, sufficient formulation will be included in order that the discussion of this analysis is better self-contained and of value, if a comprehensive review of the analysis is desired. For details of particular calculations, reference can be made to either the appendices of this report or the progress reports.

3.1 Electrode Design Analysis: In designing the electrode configuration, there are two considerations to keep in mind:

1. The electrode configuration must be capable of generating a highly uniform field. The degree of uniformity required will depend on the gaging accuracy desired, and we saw as a result of the analysis of the ideal case that the degree of uniformity must be high.

2. The electrode configuration should conform to one of a class of symmetrical arrangements on the tank boundary, which will allow the use of field rotation techniques to reduce the effects of dielectric shielding, if required.

These two considerations specify the type of problem to be solved. The first consideration requires that the physical characteristics of the electrodes (number of electrodes, their sizes, shapes, and orientations) and the potentials applied to them, must be chosen in a way that results in optimum field uniformity.

The second consideration limits this choice by imposing certain restrictions on the possible electrode shapes and orientations. For example, if complete field rotation about the tank axis is to be used, then each electrode must be of the same width, the width being dependent on the number of electrodes used. The number of electrodes must be even and they must be distributed about the tank circumference with equal spacing. If simple averaging in only two (orthogonal) directions is to be used, then the electrodes must be disposed symmetrically about the 45° axis between the two field directions. For this case, only certain pairs of electrodes must have equal widths. However, by an appropriate arrangement of the electrodes in the first case, the symmetry of the second case can be achieved as well. Therefore, in the design analysis, the condition that all electrodes have equal widths is imposed.

It should be mentioned at this point that if averaging is not to be used, then the equal width condition is an undesirable one because, for a given number of electrodes, it does not lead to a field of optimum uniformity. For a field which is to be held fixed in one direction, the best uniformity is obtained when the electrodes have decreasing width with decreasing magnitude of potential, so that the electrode array has 180° symmetry about the tank axis.

In view of the fact that a fixed field, however uniform, cannot compensate errors introduced by shielding effects, it was deemed wise to design the electrode configuration assuming that field averaging might eventually have to be used. This was done in spite of the restriction it imposes on the initial field uniformity. In essence, a practical approach was taken in which the resulting design would be an optimum trade-off among field uniformity, insensitivity to propellant orientation, and simplicity of practical hardware.

3.2 Mathematical Model: The major step in the design analysis was the determination of a suitable mathematical model of the gaging system which was conducive to theoretical analysis and which would ultimately lead to a definition of the basic electrode configuration. At the outset, it was hoped that the actual system could be analyzed in detail without approximations; however, a preliminary analysis[1] showed that this was analytically difficult and, therefore, an unattractive approach.

The realization of this fact led us to develop an approximate two dimensional model which turned out to be amenable to conventional techniques of analysis. In the establishment of a tractable model, it was borne in mind that the basic features must approximate the actual case very closely in order to determine the design parameters accurately. Furthermore, an accurate model was necessary to insure a valid performance evaluation of the gage when used in analyzing the effects of propellant distribution, shape, etc., later in the program. The approximations made in establishing the model turned out to be extremely valid; and, as a result, the model is an excellent representation of the actual case.

As a result of this fortuitous situation, a calculus of variations technique could be used to determine the required electrode sizes, positions, and potentials, which are necessary to produce internal fields of optimum uniformity. In fact, the general case of N electrodes was completely solvable. This was the outcome hoped for, and it led to closed form expressions for the desired design parameters (electrode sizes and potentials).

(1) Monthly Progress Report; August, 1966.

Because of the basically cylindrical nature of the tank, the two dimensional model depicted in Figure (III-1) was determined to be the desired one. The model differs from the actual tank in two ways. First, this particular model (tank cross-section) implies that the tank is a very long cylinder and neglects the end caps. Second, the model does not include the insulating layer between the electrodes and the grounded tank wall. It can be shown[2] that the insulation does not appreciably influence the field inside the electrode boundary since its thickness is small compared to the tank radius. In three dimensions, the electrodes are long, parallel conducting strips of equal widths.

3.3 Optimization of Field Uniformity: The method used for determining the desired discrete electrode configuration which produces a field of optimum uniformity is based on a standard calculus of variations technique. The usefulness of this technique is made clear by the following considerations:

Let us assume that we place N equal width (angular width = 2α) equally spaced electrodes on the tank boundary (a configuration which would allow averaging) and apply to each of these electrodes a fixed potential V_K, which may be different for each electrode. As an example, the distribution of electrode potentials at the tank wall might look like that depicted in Figure (III-2). Now this potential will establish a unique field pattern within the tank. If we change any of the potentials V_K or change the widths or spacings of the electrodes, the field pattern inside the tank will experience a corresponding change. The object of the design analysis, therefore, is to vary (mathematically) all of these electrode parameters until the field pattern becomes the most uniform. For a fixed number of electrodes on the boundary there will correspond a best electrode

(2) Loc. Cit.

width, spacing, and potential distribution which results in optimum field uniformity. Clearly, this uniformity will become more nearly perfect as the number N of electrodes is increased, since in the limit of an infinite number of electrodes (with a cos θ potential distribution) the field becomes perfectly uniform.

The mathematical technique for handling an optimization problem of this type is the following: First, we analytically determine the potential function $\phi_N(r,\theta)$ that would exist inside the tank due to N equal width electrodes symmetrically positioned on the tank wall. This determination requires the solution of Laplace's equation (polar coordinates):

$$\nabla^2 \phi_N = \frac{\partial}{\partial r}\left(r \frac{\partial \phi_N}{\partial r}\right) + \frac{1}{r} \frac{\partial^2 \phi_N}{\partial \theta^2} = 0 \qquad (3.1)$$

Inside the circular region of Figure (III-1), subject to the N-electrode boundary potential profile $V(\theta)$ illustrated in Figure (III-2). The general form of $\phi_N (r, \theta)$ for these cases will be

$$\phi_N (r, \theta) = \sum_{m=1}^{\infty} \left(A_m r^m \sin m\theta + B_m r^m \cos m\theta\right). \qquad (3.2)$$

where the coefficients A_m and B_m are determined by the particular boundary potential function $V(\theta)$ through the usual Fourier relations,

$$A_m = \frac{1}{\pi a^m} \int_{-\pi}^{\pi} V(\theta) \sin m\theta d\theta \qquad (3.3)$$

and

$$B_m = \frac{1}{\pi a^m} \int_{-\pi}^{\pi} V(\theta) \cos m\theta d\theta \qquad (3.4)$$

where a is the tank radius.

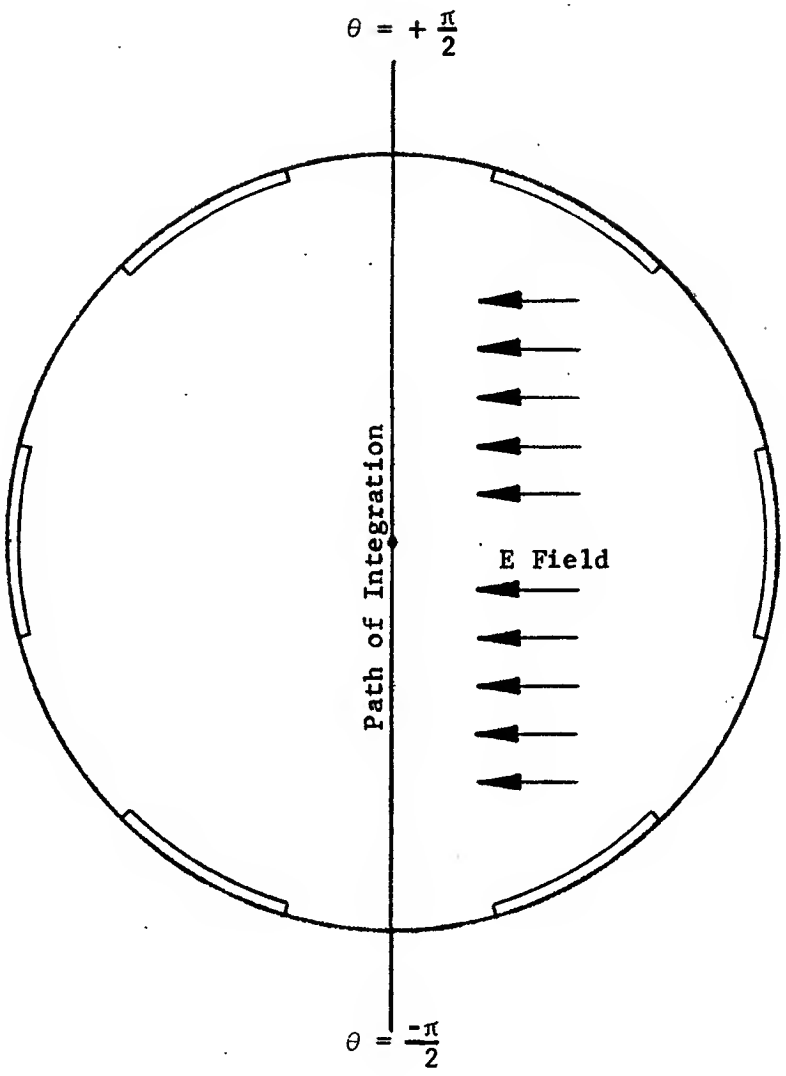

Figure III-1

Cross-Section of Tank Showing Path of Integration for the evaluation of Gauss' Integral.

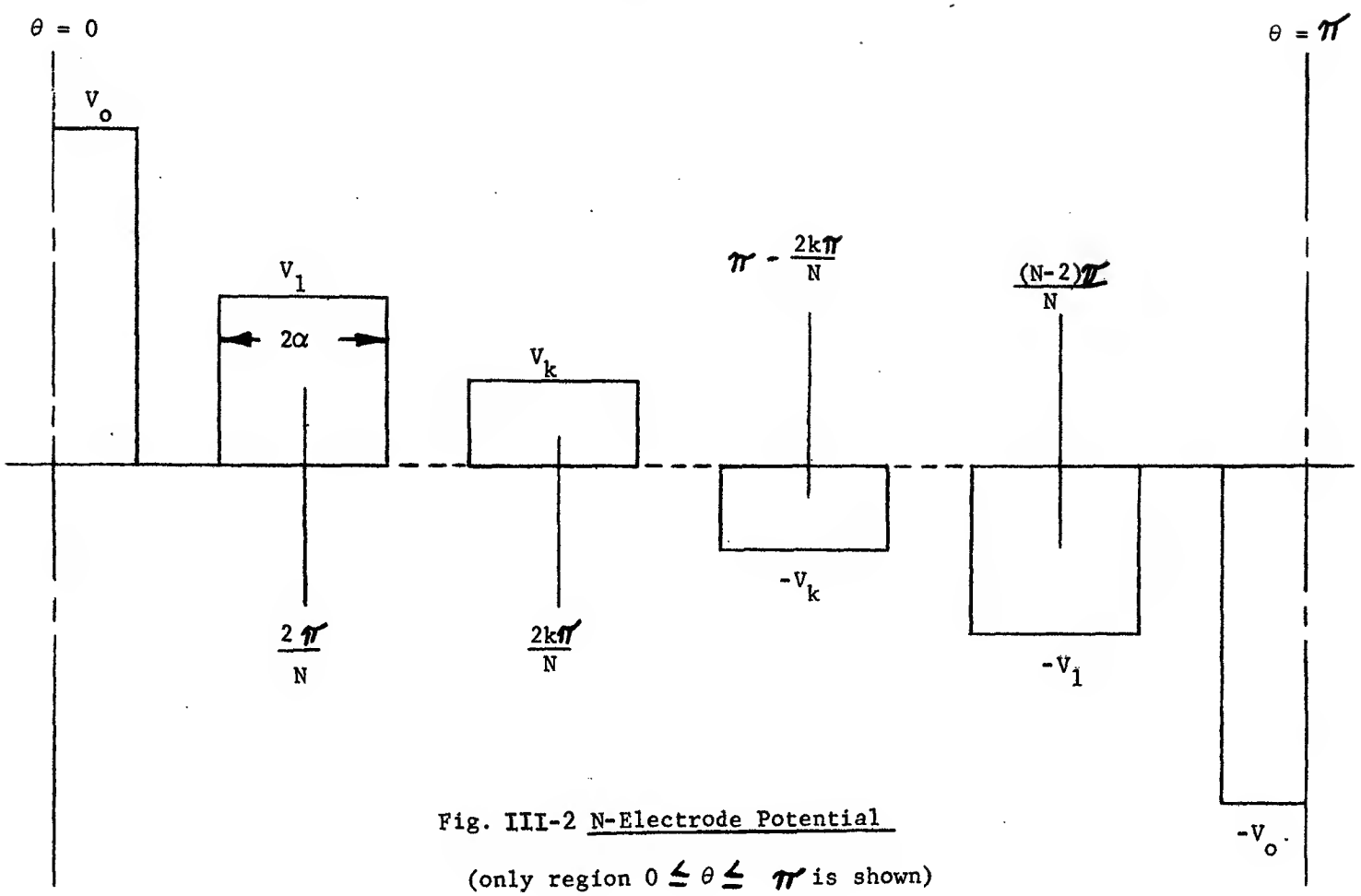

Fig. III-2 N-Electrode Potential

(only region $0 \leq \theta \leq \pi$ is shown)

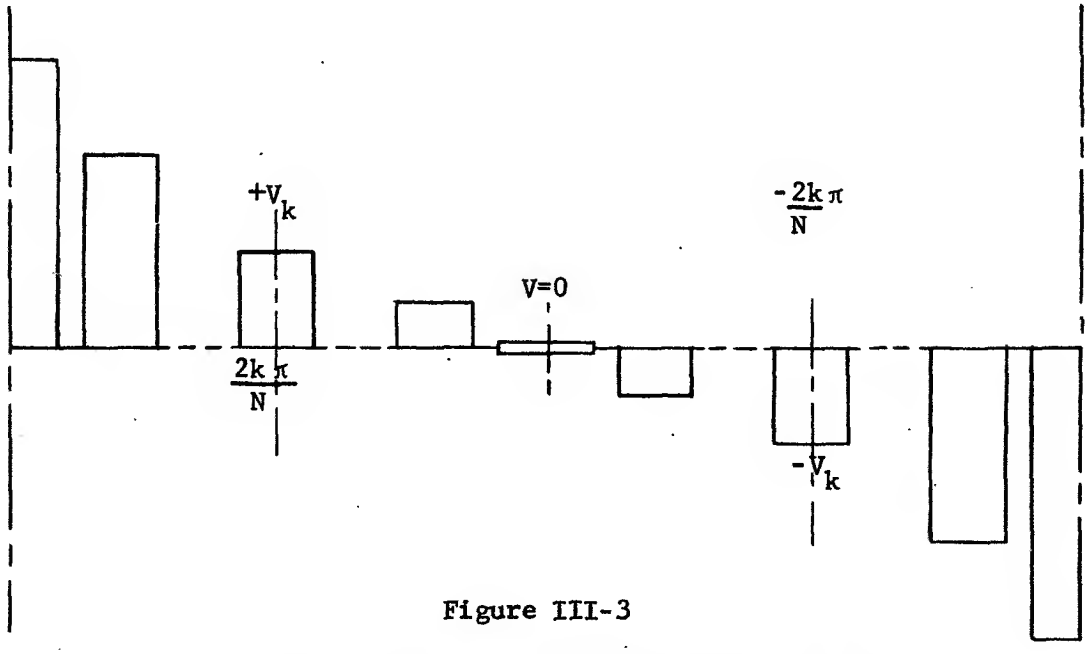

Figure III-3

Boundary Potential for Symmetry Group N=4k

Now $V(\theta)$ contains all of the information about the electrode configuration; i.e., $V(\theta)$ is also a function of electrode width 2α, the electrode positions and the individual electrode potentials V_K. Therefore, the coefficients A_m and B_m also contain this information through (3.3) and (3.4). The optimization problem, then, becomes one of adjusting the coefficients A_m and B_m in Equation (3.2) by mathematically varying each V_K and the widths α so that $\phi_N(r, \theta)$ becomes, in functional form, as close to the perfectly uniform field potential function $\phi_o = V_o \frac{r}{a} \cos\theta$, as is possible. This amounts to saying that we want to adjust the coefficients A_m and B_m so that the difference $\Delta\phi = \phi_o(r, \theta) - \phi_N(r, \theta)$ is as small as possible at each interior point (r, θ) of the tank.

To do this, we utilize the Mean Square Error Integral Function[3] defined by

$$M(\alpha, V_K) = \frac{1}{\pi a^2} \int_{-\pi}^{\pi} \int_{o}^{a} \left[\phi_o(r,\theta) - \phi_N(r,\theta,\alpha,V_k) \right]^2 r\,dr\,d\theta. \qquad (3.5)$$

This integral gives the squared difference of ϕ_o and ϕ_N at each interior point (r, θ) averaged over the domain of interest. By minimizing this with respect to the variable design parameters α and V_k in ϕ_N; i.e.,

$$\frac{\partial M}{\partial \alpha} = 0; \quad \frac{\partial M}{\partial V_k} = 0 \text{ (for each k)} \qquad (3.6)$$

we can determine the values of α and V_k which give the greatest uniformity. In fact, the method is completely analogous to a "least squares fit" of ϕ_N to ϕ_o. The calculation of this integral for specific electrode configurations is the primary concern in the electrode design analysis.

---

(3) See Appendix B for a discussion of this technique.

To calculate the Mean Square Error Function of Equation (3.5) we need the explicit form of the interior potential $\phi_N(\alpha, V_K, r, \theta)$.

3.4 Determination of ϕ_N: In this section, we present the results of the derivation of the interior potential function $\phi_N(r,\theta,\alpha,V_k)$ due to N electrodes symmetrically positioned on the boundary r = a. Each electrode is assumed to have an angular half width, α. The electrodes occur in pairs; one with applied voltage $+V_k$, the other with $-V_k$. As we will see, the magnitudes of the voltages V_k approximate a $\cos\theta$ variation around the boundary.

Before writing down the results for ϕ_N, a point concerning the symmetry of the electrode configuration should be made. Since the electrodes must occur in pairs, the number of electrodes (N) must be an even integer. Now these can be broken down into two distinct symmetry groups; one designated,

$$N = 4k + 2;\ k = 0, 1, 2, 3 \ldots\ldots$$
$$= 2, 6, 10, 14 \ldots\ldots$$

and the other,

$$N = 4k;\ k = 1, 2, 3 \ldots\ldots$$
$$= 4, 8, 12, 16 \ldots\ldots$$

The first group has field rotational symmetry, but not 45° symmetry. The second possesses both. In addition, the second group can be further divided into two subgroups. The distinction here is one of electrode orientation; whether a gap or electrode appears at the boundary point $\theta = \frac{\pi}{2}$. The subgroups can be transformed into each

other by rotating the electrode system through an angle $\frac{\pi}{N}$. In the derivations of ϕ_N both groups were considered, resulting in an expression ϕ_N for each case.

The appropriate N electrode boundary potential profile for the N = 4K+2 symmetry group is depicted in Figure (III-2), and the one for the N = 4K group is shown in Figure (III-3).

The solution of Laplace's equation (3.1) inside the region of Figure (III-1), subject to these boundary conditions, leads to the following explicit forms for $\phi_N(r, \theta, \alpha, V_K)$. For N = 4K + 2:

$$\phi_N(r,\theta,\alpha,V_k) = \frac{4}{\pi}\sum_{m=1}^{\infty}\left(V_0 + 2\sum_{K=1}^{\frac{N-2}{4}} V_K \cos\frac{2mk\pi}{N}\right)\left(\frac{r}{a}\right)^m \frac{\sin m\alpha}{m}\cos m\theta \qquad (3.7)$$

For N = 4K:

$$\phi_N(r,\theta,\alpha,V_K) = \frac{4}{\pi}\sum_{m=1}^{\infty}\left(V_0 + 2\sum_{K=1}^{N/4} V_K \cos\frac{2mk\pi}{N}\right)\left(\frac{r}{a}\right)^m \frac{\sin m\alpha}{m}\cos m\theta \qquad (3.8)$$

In both of these expressions, the index m takes on only odd values.

It is to be noted that the only difference in these two expressions is in the upper limit of the k sum. Therefore, in the remaining calculations we will not distinguish between the two cases. The only time that this is necessary is when an explicit writing out of the expressions is required. We will not have occasion to do this in the following discussions.

3.5 Calculation of the Mean Square Error Integral Function: With the expression for ϕ_N given by (3.7) or (3.8), and using the uniform field potential $\phi_o(r, \theta) = V_a \frac{r}{a} \cos\theta$, the Mean Square Error Integral Function (3.5) can be calculated. Without doing the tedious computation in detail, the result is:

$$M(\alpha, V_K) = V_o^2 \left[\frac{1}{4} - \frac{1}{2} A_1(N) \sin\alpha + \frac{1}{2} \sum_{m=1}^{\infty} A_m^2(N) \frac{\sin^2 m\alpha}{m^2(m+1)} \right] \qquad (3.9)$$

where the coefficients $A_1(N)$ and $A_m^2(N)$ are given by the complicated series expressions

$$A_1(N) = \frac{4}{\pi} \left(\frac{V_o}{V_a} + 2 \sum_{k=1} \frac{V_K}{V_a} \cos \frac{2K\pi}{N} \right) \qquad (3.10)$$

and (introducing new summation indices to avoid confusion)

$$A_m^2(N) = \frac{16}{\pi^2} \left[\left(\frac{V_o}{V_a} \right)^2 + 4 \frac{V_o}{V_a} \sum_{r=1} \frac{V_r}{V_a} \cos \frac{2mr\pi}{N} + 4 \sum_{s=1} \sum_{t=1} \frac{V_s V_t}{V_a^2} \cos \frac{2ms\pi}{N} \cos \frac{2mt\pi}{N} \right] \qquad (3.11)$$

In all of the sums appearing in these coefficients, the upper limits are either $\frac{N-2}{4}$ or $\frac{N}{4}$, as in the $\emptyset_N$ expressions. Because of the complicated expression for M (α, V_K) we will not attempt any explicit evaluations. In the actual analysis, each of the trigonometric series appearing in M were evaluated in closed form, so that numerical evaluation of the series could be performed easily. However, these evaluations are not necessary here as we will see below.

3.6 Variational Procedure for Determining α and V_K: To determine the optimum design parameters α and V_K, the expression for M appearing in (3.9) must be minimized, as we have stated; i.e., we must compute:

$$\frac{\partial M}{\partial \alpha} = 0; \quad \frac{\partial M}{\partial V_K} = 0$$

This leads to a set of simultaneous equations in the unknowns α and V_K, the solutions of which give the desired values of these parameters. Without details, we write out the resulting simultaneous equations:

$$\text{For } \frac{\partial M}{\partial \alpha} = 0,$$

$$A_1(N)\cos\alpha - \sum_{m=1}^{\infty} A_m^2(N)\,\frac{\sin 2m\alpha}{m(m+1)} = 0 \tag{3.12}$$

For $\frac{\partial M}{\partial V_K} = 0$, and for each K = 0, 1, 2 ...., $\frac{N-2}{4}$ or $\frac{N}{4}$.

$$\cos\frac{2k\pi}{N}\sin\alpha - 2\sum_{m=1}^{\infty} A_m(N)\cos\frac{2mk\pi}{N}\,\frac{\sin^2 m\alpha}{m^2(m+1)} = 0 \tag{3.13}$$

The set of simultaneous equations (3.12) and (3.13) are the important relations for determining the required design parameters and V_K. The error function (3.9) is the expression by which we are able to judge how uniform the resulting field will be; and, therefore, it is used to determine the number of electrodes necessary to achieve a desired uniformity.

3.7 Design Analysis Conclusions: If equations (3.12) and (3.13) are solved for the cases of N = 2, 4, 6, etc., an unphysical solution occurs for the electrode width α in all cases of N greater than 2. The achievement of a minimum in the mean square error requires, in these cases, that the electrodes be slightly overlapped. However, since this is physically impossible, the conclusion to be drawn from this is that M cannot be completely minimized. The smallest value of the error function is obtained when all electrodes are butted edge to edge; i.e.,

$$\alpha = \pi/N \tag{3.14}$$

Furthermore, the corresponding condition on the applied potentials V_K can be shown to be:

$$V_K = V_o \cos \frac{2K\pi}{N} \tag{3.15}$$

Therefore, the first conclusion of the theoretical design analysis is that, for a given number of electrodes, optimum uniformity is achieved if the entire circumference of the tank wall is covered by the electrode array, leaving very small interelectrode spacing. The second conclusion, which is a bit surprising, especially for a small number of electrodes, is that the potentials which are to be applied follow the $V_o \cos\theta$ relation exactly; the proper value of V_K being determined by the angular position of the center of the conductor strip.

Although these conclusions seem evident in retrospect, they could not be obtained justifiably with any degree of certainty before the calculations were made. For example, instead of computing the mean square error over the volume of the tank, one could have computed it over the tank circumference, in an attempt to fit a discrete step potential function most closely to the continuous $\cos\theta$ one at the boundary. A calculation of this leads to the same conclusions concerning the butting of electrodes but the conditions on the V_K are significantly different. An analysis of this difference leads to the conclusion that the second choice results in an optimization of field uniformity near the tank wall but results in a bad field uniformity in the tank center. In a following section, we will show that the volume error approach is the correct one since the field uniformity throughout the tank increases at every point with an increase in the number of electrodes, as it should.

3.8 Number of Electrodes: The remaining determination to be made in the analysis is the number of electrodes required to make the deviations from perfect field uniformity small. To determine this, we simply compute the values of M in Equation (3.9) as a function of N, using the relations for α and V_K expressed in Equations (3.14) and (3.15).

The result of such a calculation is depicted in the bar graph of Figure (III-4). In the graph, the RMS error ($\pm\sqrt{M_N}$) is plotted for the cases of N = 2,4,6,8,12, and 16 electrodes. The error is normalized to be a percentage of V_o (which is the largest potential appearing on the electrode boundary) and is, therefore, a plot of $\pm\sqrt{M_N/V_o}$ versus N.

It is noticed that the expected improvement with increasing N occurs for $N > 2$, but for N = 2 there is an apparent anomally in this trend.

This can be explained as follows: In the cases of $N > 2$ (the cases which involve more than a single pair of electrodes) the restriction of requiring equal plate sizes reduces the degrees of freedom by which M_N can be minimized. In other words, if the plate sizes were to be adjusted also, lower values of M_N would result as compared to the results obtained above. In the minimization process for two electrodes, however, the adjustment on α is automatically the more complete variation, and so a much lower value of M_2 results. The equivalent restriction of equal plate size for N = 2 would be to fix each plate size at $\alpha = 90^o$ (the two plates touching) which would obviously give a result worse than the others, and thus, in keeping with the expected trend. In essence, the case of two electrodes which

we have calculated is not in the same class as the others. In fact, this case can be viewed as an N = 4 configuration, in which we have optimized the four plate widths as well. In so doing, the RMS value is halved. Even though a variation of individual plate widths can lead to lower values of M_N for the same number of electrodes, as we have stated, it does not leave an electrode configuration which is amenable to field rotation techniques. This latter symmetry consideration is the original reason for placing the restriction of equal electrode widths. The important conclusion to be derived from this calculation is that the convergence of the field to a highly uniform configuration is very rapid. A more comprehensive way of examining the resulting field homogeneity is to investigate its variations inside the tank.

3.9 Evaluation of Electric Field Uniformity Inside the Tank: In this section, we endeavor to determine just how uniform the field is inside the tank as a result of optimizing the electrode design parameters. We can do this by evaluating the mean square error integral for various regions of the tank using the optimum electrode design parameters obtained from above. We know in advance that the RMS deviation of the true potential from ideal should be much smaller near the axis of the tank than at the tank walls where the potential is distorted by the discrete geometry of the electrodes. However, it is of interest to see how large an internal region possesses an RMS deviation which is below, say, 1%.

To do this, we simply calculate $\tilde{M}_N = \frac{M_N}{V_o^2}$ over an area of πr^2. Upon doing this, the expression for $\tilde{M}_N(r)$ is:

$$\tilde{M}_N(r) = \left(\frac{1}{4} - \frac{1}{2} A_1 \sin\alpha\right) \cdot \left(\frac{r}{a}\right)^2 + \frac{1}{2} \sum_{m=1}^{\infty} A_m^2 \left(\frac{r}{a}\right)^{2m} \frac{\sin^2 m\alpha}{m^2(m+1)} \qquad (3.16)$$

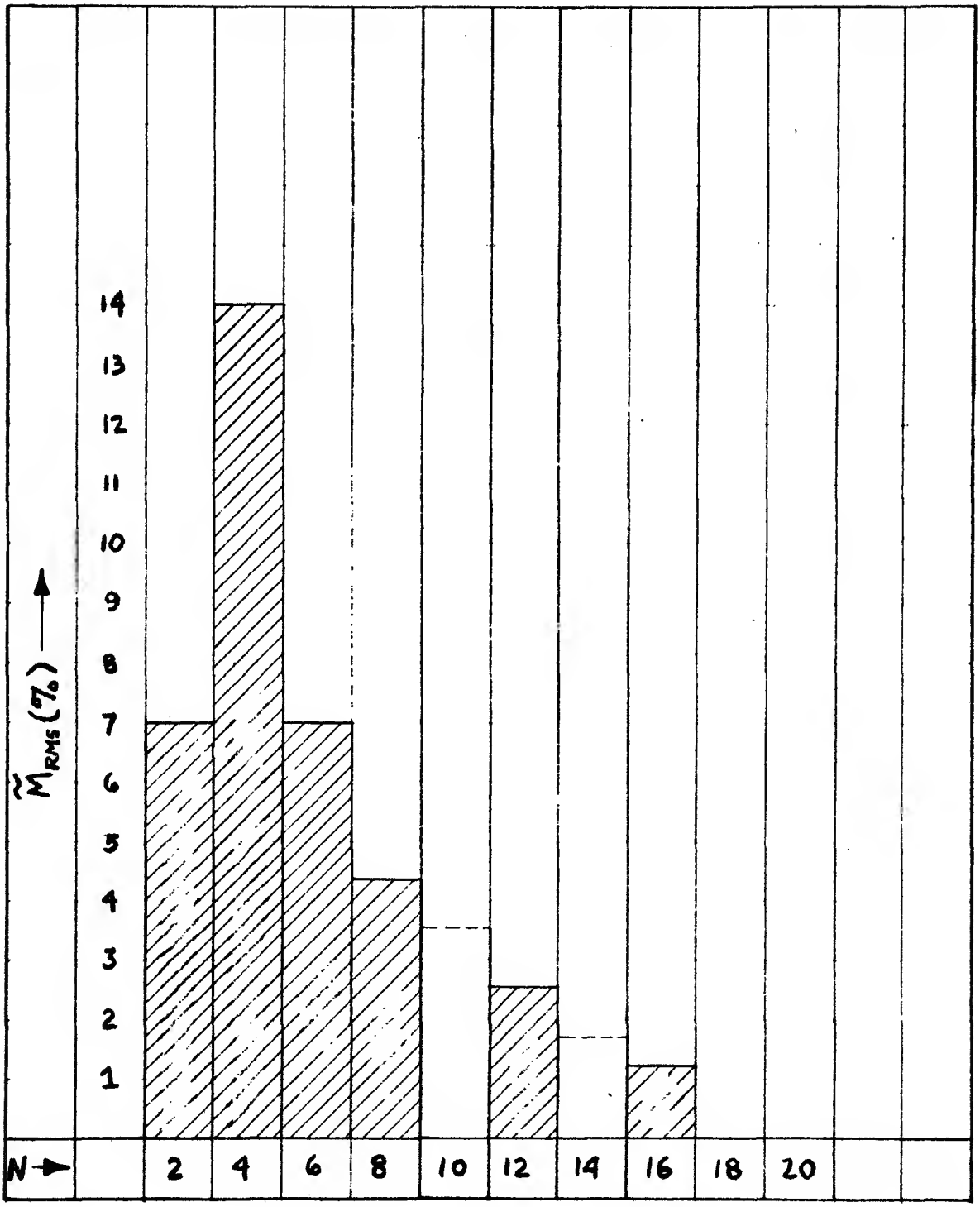

Figure III-4

Total RMS Error vs Number of Electrodes

where A_1 and A_m^2 are the same coefficients as before, a is the tank radius and α is the optimum electrode half-width. The RMS value is then simply $\sqrt{\widetilde{M}_N(r)}$. In Figure (III-5) we have plotted the RMS value as a function of r for the various cases of N. The plot for N = 2 is the best obtainable one, in the sense of our previous discussions.

The results of this calculation show that the uniformity is extremely good over most of the tank volume for the cases where $8 \leq N \leq 20$. For eight electrodes, the RMS deviation from perfect uniformity is less than 1% over the radial range $0 \leq \frac{r}{a} \leq 0.81$, which corresponds to 67% of the cylindrical tank volume. For twelve electrodes, the RMS deviation of the field from ideal is less than 1% over more than 80% of the cylindrical tank volume. For sixteen electrodes, the same homogeneity can be achieved over more than 98% of the tank volume. Extrapolating these results to 20 electrodes, definitely concludes that the RMS homogeneity for this case will be better than 1% over the entire tank volume. This case would then represent an upper limit on the number of electrodes required to produce sufficient field uniformity.

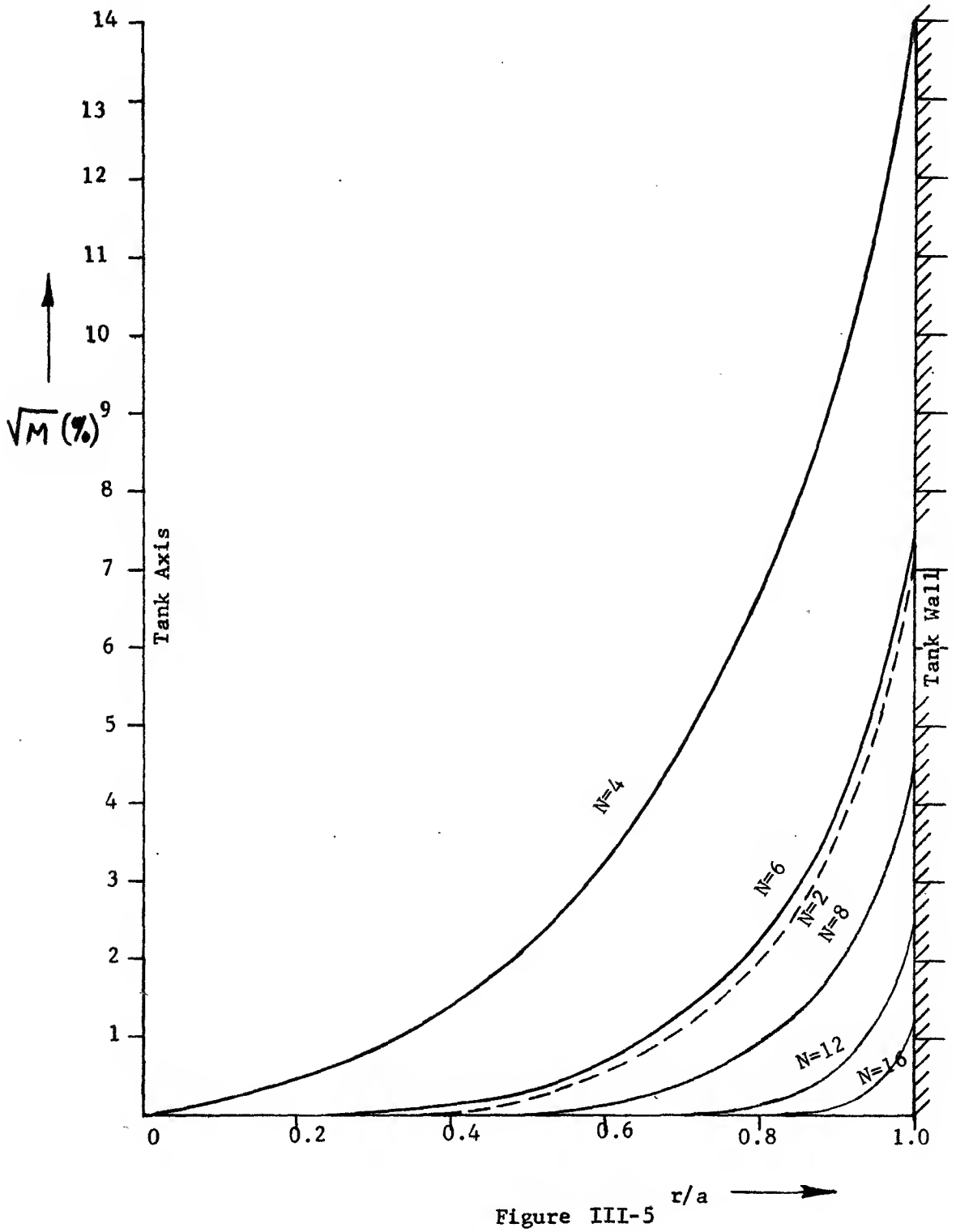

Figure III-5

RMS Homogeneity Inside Tank

IV. THEORETICAL PERFORMANCE ANALYSIS

4.1 Calculation of System Capacitance (Empty Tank): In this section we turn our attention to the calculation of the general N-electrode gage capacitance assuming empty tank conditions.

The general procedure is to calculate Gauss' integral along the line $\theta = \pm\frac{\pi}{2}$; refer to Figure (IV-1). This integral gives the magnitude of the total charge Q per meter residing on the electrodes. The required integral is

$$|Q| = \epsilon_o \int_o^a \left[E_\theta \left(\theta = \frac{\pi}{2}\right) - E_\theta \left(\theta = -\frac{\pi}{2}\right) \right] dr; \tag{4.1}$$

where E_θ is the θ component of the interior electric field evaluated along $\theta = \pm\frac{\pi}{2}$. By symmetry, $E_\theta(\theta=-\frac{\pi}{2}) = -E_\theta(\theta=\frac{\pi}{2})$ so (1.4) becomes

$$|Q| = 2\epsilon_o \int_o^a E_\theta \left(\theta = \frac{\pi}{2}\right) dr \tag{4.2}$$

E_θ can be computed from the N-electrode potential $\phi_N(r,\theta)$ by

$$E_\theta = -\frac{1}{r}\frac{\partial \phi_N}{\partial \theta}, \tag{4.3}$$

The form of ϕ_N is given by (3.7) so E_θ, evaluated at $\theta = \frac{\pi}{2}$, is

$$E_\theta\left(\theta = \frac{\pi}{2}\right) = \frac{4}{\pi} \sum_{m=1}^{\infty} \left(V_o = 2\sum_k V_k \cos\frac{2mk\pi}{N}\right) \frac{r^{m-1}}{a^m} \sin m\alpha \sin\frac{m\pi}{2} \tag{4.4}$$

Therefore, evaluating the integral in (4.2) gives,

$$|Q_N| = \frac{8\epsilon_o}{\pi} \sum_{m=1}^{\infty} \left(V_o + 2\sum_k V_k \cos\frac{2mk\pi}{N}\right) \frac{\sin m\frac{\pi}{2} \sin m\alpha}{m} \tag{4.5}$$

This total charge is equivalent to the sum of the individual charges on each pair of plates; i.e.,

$$|Q_N| = |Q_o| + \sum_k |Q_k| \tag{4.6}$$

We can now identify each of these individual charges as

$$|Q_o| = \frac{8\epsilon_o V_o}{\pi} \sum_{m=1}^{\infty} \frac{\sin\frac{m\pi}{2}\sin m\alpha}{m}, \tag{4.7}$$

and for each plate pair designated by k

$$|Q_k| = \frac{16\epsilon_o V_k}{\pi} \sum_{m=1}^{\infty} \frac{\cos\frac{2mk\pi}{N}\sin\frac{m\pi}{2}\sin m\alpha}{m} \tag{4.8}$$

The series appearing in (4.7) and (4.8) can be computed in closed form, and are

$$\sum_{m=1}^{\infty} \frac{\sin\frac{m\pi}{2}\sin m\alpha}{m} = \frac{1}{4}\ln\left(\frac{1+\sin\alpha}{1-\sin\alpha}\right) \tag{4.9}$$

and

$$\sum \frac{\cos\frac{2mk\pi}{N}\sin\frac{m\pi}{2}\sin m\alpha}{m} = \frac{1}{8}\ln\left(\frac{\left[1+\sin\left(\frac{2k\pi}{N}+\alpha\right)\right]\left[1-\sin\left(\frac{2k\pi}{N}-\alpha\right)\right]}{\left[1+\sin\left(\frac{2k\pi}{N}-\alpha\right)\right]\left[1-\sin\left(\frac{2k\pi}{N}+\alpha\right)\right]}\right) \tag{4.10}$$

The capacitance for each pair of plates is computed by

$$C_o = \frac{|Q_o|}{2V_o} \tag{4.11}$$

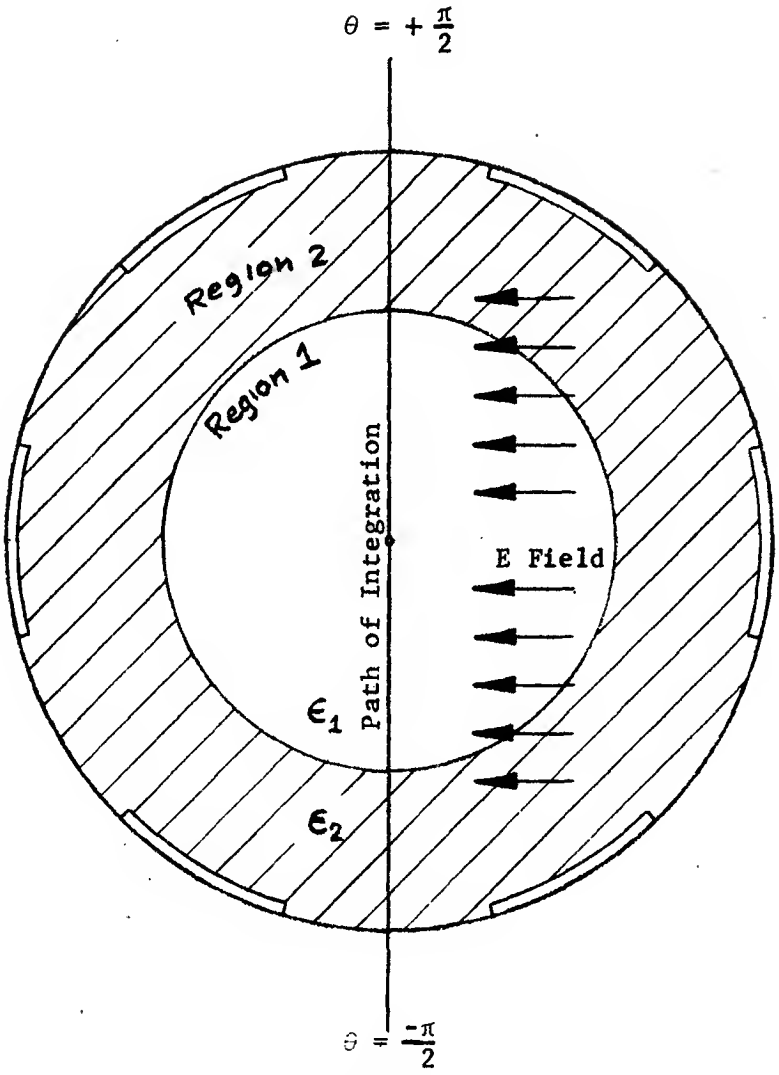

Figure IV-1

Cross-Section of Tank Showing Path of Integration for the evaluation of Gauss' Integral.

and for each k by,

$$C_k = \frac{|Q_k|}{2V_k} \quad . \tag{4.12}$$

Thus, the N-electrode capacitance C_N is just the parallel combination of C_o and the C_k's or

$$C_N = C_o + \sum_k C_k ; \tag{4.13}$$

where the upper limit on k sum is either $\frac{N-2}{4}$ or $\frac{N}{4}$ depending on which electrode symmetry group applies. Combining all of these expressions gives the general expression for the empty tank capacitance of an N-electrode gage.

$$C_N = \frac{\varepsilon_o}{\pi} \left\{ \ln\left(\frac{1+\sin\alpha}{1-\sin\alpha}\right) + \sum_{k=1} \ln \left(\frac{\left[1+\sin\left(\frac{2k\pi}{N}+\alpha\right)\right]\left[\left(1-\sin\left(\frac{2k\pi}{N}-\alpha\right)\right]\right.}{\left[1+\sin\left(\frac{2k\pi}{N}-\alpha\right)\right]\left[1-\sin\left(\frac{2k\pi}{N}+\alpha\right)\right]} \right) \right\} \tag{4.14}$$

4.2 Analysis of Error Due to Fluid Configuration: In this section, we present an analysis of the effects of fluid configuration on the system capacitance. To do this we have considered a propellant/vapor configuration in which the liquid/vapor interface is a cylindrical surface, internally concentric with the tank wall. This can be made to represent two different configurations of the propellant when the fluid and vapor portions are interchanged (see Figure IV-1). This configuration is, of course, an idealization but it does represent an important case because it possesses a symmetry which is completely immune to error reduction by orthogonal averaging techniques. As a result, the case is one in which the dielectric shielding effects cannot be reduced.

In the following analysis, we will derive the expression for the capacitance of the general N-electrode gage as a function of the propellant mass present in the tank. By so doing, we can compute the error in the measured capacitance of the two configurations for any amount of fuel in the tank, by subtracting the two results.

We begin by solving Laplace's equation for the potential in each of the regions (1) and (2). The dielectric constants for these regions are ϵ_1 and ϵ_2, respectively. The general expressions for the electric potentials in these regions are then given by,

$$\phi_1(r, \theta) = \sum_m \tau_m \, r^m \cos m\theta \tag{4.15}$$

$$\phi_2(r, \theta) = \sum \sigma_m(r) \cos m\theta \tag{4.16}$$

where,

$$\sigma_m(r) = \alpha_m \, r^m + \beta_m \, r^{-m} \tag{4.17}$$

The task now is to determine the coefficients τ_m, α_m, and β_m from the appropriate boundary conditions at the dielectric interface (r = b) and at the tank wall (r = a). At the dielectric interface we must satisfy the conditions that the tangential component (E_θ) of the electric field is continuous across the boundary (at r = b); i.e.,

$$E_{\theta_1} (r = b) = E_{\theta_2} (r = b) \tag{4.18}$$

and that the normal component of the displacement field ($D_r = \epsilon E_r$) is continuous. Therefore,

$$E_{r_1}(r = b) = \frac{\epsilon_2}{\epsilon_1} E_{r_2}(r = b) \tag{4.19}$$

Using (4.15) and (4.16), the θ components of the fields at the interface are given by

$$E_{\theta_1}(r = b) = -\left(\frac{1}{r}\frac{\partial \phi_1}{\partial \theta}\right)_{r=b} = \sum_{m=1}^{\infty} m \tau_m b^{m-1} \sin m\theta \tag{4.20}$$

and,

$$E_{\theta_2}(r = b) = -\left(\frac{1}{r}\frac{\partial \phi_2}{\partial \theta}\right)_{r=b} = \sum_{m=1}^{\infty} m(\alpha_m b^{m-1} + \beta_m b^{-(m+1)}) \sin m\theta \tag{4.21}$$

From these, Equation (4.18) is satisfied if

$$\tau_m - \alpha_m - \beta_m b^{-2m} = 0 \tag{4.22}$$

Similarly, by computing $E_r = -\frac{\phi}{r}$ from (4.15) and (4.16) and satisfying (4.19) gives

$$\tau_m - \frac{\epsilon_2}{\epsilon_1}(\alpha_m - \beta_m b^{-2m}) = 0 \tag{4.23}$$

Now at $r = a$, $\phi_2(a, \theta)$ must satisfy the N-electrode boundary condition which we calculated in a previous report. Therefore,

$$\alpha_m a^m + \beta_m a^{-m} = \sigma_m(a) \tag{4.24}$$

where,

$$\sigma_m(a) = \frac{4}{\pi} \frac{\sin m\alpha}{m} \left[V_o + 2 \sum_{k=1} V_k \cos \frac{2mk\pi}{N} \right] \tag{4.25}$$

Equations (4.22), (4.23), and (4.24) constitute the three simultaneous equations necessary for determining τ_m, α_m, and β_m. Solving these we obtain:

$$\tau_m = \frac{2a^m \sigma(m)}{a^{2m}(1 + \frac{\epsilon_1}{\epsilon_2}) + b^{2m}(1 - \frac{\epsilon_1}{\epsilon_2})} \tag{4.26}$$

$$\alpha_m = \frac{(1 + \frac{\epsilon_1}{\epsilon_2})\, a^m \sigma(m)}{a^{2m}(1 + \frac{\epsilon_1}{\epsilon_2}) + b^{2m}(1 - \frac{\epsilon_1}{\epsilon_2})} \tag{4.27}$$

$$\beta_m = \frac{(1 - \frac{\epsilon_1}{\epsilon_2})\, a^m b^{2m} \sigma(m)}{a^{2m}(1 + \frac{\epsilon_1}{\epsilon_2}) + b^{2m}(1 - \frac{\epsilon_1}{\epsilon_2})} \; ; \tag{4.28}$$

where, as before (Equation 4.25), $\sigma(m) = \sigma_m(a)$.

With the coefficients τ_m, α_m, and β_m evaluated we can now compute the capacitance of the gage as a function of the propellant mass present. This calculation is completely analogous to the one performed in the last report where we first determined the charge on the plates by evaluating Gauss' integral along the line $\theta = \pm \pi/2$. Because of the two regions, the magnitude of the plate charge is expressed as

$$|Q| = 2 \left[\epsilon_1 \int_o^b E_{\theta_1}(\theta = \frac{\pi}{2})\, dr + \epsilon_2 \int_b^a E_{\theta_2}(\theta = \frac{\pi}{2})\, dr \right] \tag{4.29}$$

where E_{θ_1} $(\theta = \frac{\pi}{2})$ and E_{θ_2} $(\theta = \frac{\pi}{2})$ are obtained from (4.20) and (4.21) with $\theta = \frac{\pi}{2}$ and $b = r$;

$$E_{\theta_1}(\theta = \tfrac{\pi}{2}) = \sum_{m=1}^{\infty} m \tau_m r^{m-1} \sin m \tfrac{\pi}{2} \tag{4.30}$$

$$E_{\theta_2}(\theta = \tfrac{\pi}{2}) = \sum_{m=1}^{\infty} m(\alpha_m r^{m-1} + \beta_m r^{-(m+1)}) \sin m \tfrac{\pi}{2} \tag{4.31}$$

Using these expressions in (4.29) and performing the integration gives, after a little manipulation,

$$|Q| = 2 \sum_{m=1}^{\infty} \sin m \tfrac{\pi}{2} \left[(\epsilon_1 \tau_m - \epsilon_2 \alpha_m) b^m + \epsilon_2 (\alpha_m a^m - \beta_m a^{-m}) + \epsilon_2 \beta_m b^{-m}\right] \tag{4.32}$$

From Equation (4.23) we have

$$\epsilon_1 \tau_m - \epsilon_2 \alpha_m = - \epsilon_2 \beta_m b^{-2m} \tag{4.33}$$

and, therefore,

$$|Q| = 2\epsilon_2 \sum_{m=1}^{\infty} \sin \tfrac{m\pi}{2} (\alpha_m a^m - \beta_m a^{-m}) \tag{4.34}$$

Now, using the coefficients α_m and β_m from (4.27) and (4.28) we have

$$|Q| = 2\epsilon_2 \sum_{m=1}^{\infty} \sigma_m(a) \sin \tfrac{m\pi}{2} \left[\frac{1 - (\frac{b}{a})^{2m}(1 - \frac{\epsilon_1}{\epsilon_2})/(1 + \frac{\epsilon_1}{\epsilon_2})}{1 + (\frac{b}{a})^{2m}(1 - \frac{\epsilon_1}{\epsilon_2})/(1 + \frac{\epsilon_1}{\epsilon_2})}\right] \tag{4.35}$$

where $\sigma_m(a)$ is given in (4.25).

Because of the k sum appearing in $\sigma_m(a)$ we can write the total charge Q as the sum of individual charges from each pair of plates; i.e.,

$$|Q| = |Q_o| + \sum_k |Q_k| \tag{4.36}$$

Using the expression for $\sigma_m(a)$ in (4.25) we can identify each charge contribution from (4.35) and (4.36) and write the respective "geometric" capacitances* as

$$C_o = \frac{|Q_o|}{2V_o} = \frac{4\epsilon_2}{\pi} \sum_{m=1}^{\infty} \frac{\sin m\alpha \sin m\frac{\pi}{2}}{m} \left[\frac{1-(\frac{b}{a})^{2m}(1-\frac{\epsilon_1}{\epsilon_2})/(1+\frac{\epsilon_1}{\epsilon_2})}{1+(\frac{b}{a})^{2m}(1-\frac{\epsilon_1}{\epsilon_2})/(1+\frac{\epsilon_1}{\epsilon_2})} \right] \tag{4.37}$$

and for each k

$$C_k = \frac{|Q_k|}{2V_k} = \frac{8\epsilon_2}{\pi} \sum_{m=1}^{\infty} \frac{\cos\frac{2mk\pi}{N} \sin m\frac{\pi}{2} \sin m\alpha}{m} \left[\frac{1-(\frac{b}{a})^{2m}(1-\frac{\epsilon_1}{\epsilon_2})/(1+\frac{\epsilon_1}{\epsilon_2})}{1+(\frac{b}{a})^{2m}(1-\frac{\epsilon_1}{\epsilon_2})/(1+\frac{\epsilon_1}{\epsilon_2})} \right] \tag{4.38}$$

It is desirable to evaluate the trigonometric series appearing in these equations in closed form as we have done previously. However, because the coefficients in the square brackets depend on m we must employ a "trick" to make this evaluation possible. We can do this by first rewriting these coefficients in simpler form

$$\left[\frac{1-(\frac{b}{a})^{2m}(1-\frac{\epsilon_1}{\epsilon_2})/(1+\frac{\epsilon_1}{\epsilon_2})}{1+(\frac{b}{a})^{2m}(1-\frac{\epsilon_1}{\epsilon_2})/(1+\frac{\epsilon_1}{\epsilon_2})} \right] = \frac{1-Ax^m}{1+Ax^m} \tag{4.39}$$

*The geometric capacitance is the capacitance measured at the taps of the secondary of the transformer. However, the capacitance of interest is that measured on the primary side (the transformed capacitance) which we will compute.

where we have defined

$$A = (1 - \frac{\epsilon_1}{\epsilon_2}) \; / \; (1 + \frac{\epsilon_1}{\epsilon_2}) \tag{4.40}$$

and

$$x = (b/a)^2 \tag{4.41}$$

Now we can rewrite the right side of (4.39) in a series form;

$$\frac{1 - Ax^m}{1 + Ax^m} = 1 + 2 \sum_{\mu=1}^{\infty} (-Ax^m)^\mu \; . \tag{4.42}$$

Putting (4.42) into (4.37) and (4.38) gives

$$C_o = \frac{4\epsilon_2}{\pi} \left(\sum_{m=1}^{\infty} \frac{\sin \frac{m\pi}{2} \sin m\alpha}{m} + 2 \sum_{\mu=1}^{\infty} (-A)^\mu \sum_{m=1}^{\infty} \frac{x^{\mu m} \sin \frac{m\pi}{2} \sin m\alpha}{m} \right) \tag{4.43}$$

and

$$C_k = \frac{8\epsilon_2}{\pi} \left(\sum_{m=1}^{\infty} \frac{\cos \frac{2mk\pi}{N} \sin \frac{m\pi}{2} \sin m\alpha}{m} + 2 \sum_{\mu=1}^{\infty} (-A)^\mu \sum_{m=1}^{\infty} \frac{x^{\mu m} \cos \frac{2mk\pi}{N} \sin m\frac{\pi}{2} \sin m\alpha}{m} \right) \tag{4.44}$$

By employing this "trick", we have broken up the original expressions (4.37) and (4.38) into two terms each containing series in m which can now be evaluated in closed form. The evaluation of these series requires a sizeable calculation which we do not include here for reasons of brevity, and therefore simply set down the results. They are (remembering that m is restricted to odd integers only)

$$\sum_{m=1}^{\infty} \frac{x^{\mu m} \sin \frac{m\pi}{2} \sin m\alpha}{m} = \frac{1}{4} \ln \left(\frac{1 + x^{2\mu} + 2x^{\mu} \sin \alpha}{1 + x^{2\mu} - 2x^{\mu} \sin \alpha} \right) \tag{4.45}$$

and

$$\sum_{m=1}^{\infty} \frac{x^{\mu m} \cos \frac{2mk\pi}{N} \sin \frac{m\pi}{2} \sin m\alpha}{m} = \frac{1}{8} \ln \left[\frac{\left[1+x^{2\mu}+2x^{\mu}\sin\left(\frac{2k\pi}{N}+\alpha\right)\right]\left[1+x^{2\mu}-2x^{\mu}\sin\left(\frac{2k\pi}{N}-\alpha\right)\right]}{\left[1+x^{2\mu}+2x^{\mu}\sin\left(\frac{2k\pi}{N}-\alpha\right)\right]\left[1+x^{2\mu}-2x^{\mu}\sin\left(\frac{2k\pi}{N}+\alpha\right)\right]} \right] \tag{4.46}$$

The first terms in (4.43) and (4.44) can be obtained in closed form by setting x = 1 in (4.45) and (4.46).

$$C_o = \frac{\epsilon_2}{\pi} \left\{ \ln \left(\frac{1 + \sin \alpha}{1 - \sin \alpha} \right) + 2 \sum_{\mu=1}^{\infty} \left[- \frac{(1-\epsilon_1/\epsilon_2)}{(1+\epsilon_1/\epsilon_2)} \right]^{\mu} \ln \left(\frac{1 + \left(\frac{b}{a}\right)^{4\mu} + 2\left(\frac{b}{a}\right)^{2\mu} \sin \alpha}{1 + \left(\frac{b}{a}\right)^{4\mu} - 2\left(\frac{b}{a}\right)^{2\mu} \sin \alpha} \right) \right\} \tag{4.47}$$

and for each k,

$$C_k = \frac{\epsilon_2}{\pi} \left\{ \ln \left(\frac{\left[1 + \sin\left(\frac{2k\pi}{N} + \alpha\right)\right]\left[1 - \sin\left(\frac{2k\pi}{N} - \alpha\right)\right]}{\left[1 + \sin\left(\frac{2k\pi}{N} - \alpha\right)\right]\left[1 - \sin\left(\frac{2k\pi}{N} + \alpha\right)\right]} \right) + 2 \sum_{\mu=1}^{\infty} \left[- \frac{(1-\epsilon_1/\epsilon_2)}{(1+\epsilon_1/\epsilon_2)} \right]^{\mu} \ln \left(\frac{\left[1+\left(\frac{b}{a}\right)^{4\mu}+2\left(\frac{b}{a}\right)^{2\mu}\sin\left(\frac{2k\pi}{N}+\alpha\right)\right]\left[1+\left(\frac{b}{a}\right)^{4\mu}-2\left(\frac{b}{a}\right)^{2\mu}\sin\left(\frac{2k\pi}{N}-\alpha\right)\right]}{\left[1+\left(\frac{b}{a}\right)^{4\mu}+2\left(\frac{b}{a}\right)^{2\mu}\sin\left(\frac{2k\pi}{N}-\alpha\right)\right]\left[1+\left(\frac{b}{a}\right)^{4\mu}-2\left(\frac{b}{a}\right)^{2\mu}\sin\left(\frac{2k\pi}{N}+\alpha\right)\right]} \right) \right\} \tag{4.48}$$

The total N-electrode geometric capacitance can then be determined from

$$C_N = C_o + \sum_{k=1}^{\frac{N}{4} \text{ or } \frac{N-2}{4}} C_k \tag{4.49}$$

In (4.47) and (4.48) the square of the ratio b/a is proportional to the fractional propellant mass present in a cylindrical tank when the liquid is in region (1) and proportional to one minus the fractional mass when the liquid is in region (2); i.e., the fractional mass in the first case is given by (for a tank cylinder of length L and radius a, and cylindrical fuel "slug" of length L radius b, and density ρ),

$$\frac{m}{M} = \frac{\pi b^2 L\rho}{\pi a^2 L\rho} = \left(\frac{b}{a}\right)^2 \tag{4.50}$$

In the second case we have,

$$\frac{m}{M} = \frac{(\pi a^2 - \pi b^2)\, L\rho}{\pi a^2\, L\rho} = 1 - \left(\frac{b}{a}\right)^2 .$$

or

$$\left(\frac{b}{a}\right)^2 = 1 - \frac{m}{M} . \tag{4.51}$$

Also, in evaluating the capacitance of either of the two different configurations of fuel we must correctly identify ϵ_1 and ϵ_2. With these changes Equations (4.47), (4.48), and (4.49) can be used for both cases.

As we mentioned, the expressions (4.47), (4.48), and (4.49) are the "geometric" capacitances of the gage and do not represent the true measurable capacitances of the gage. This latter capacitance is called the transformed capacitance, and is the capacitance measured on the primary side of the transformer. It is different from the geometric capacitance because the N-electrode gage is viewed as an equivalent single parallel plate capacitor on the primary side; the geometric capacitance of each pair of plates is transformed differently because of the difference in the transformer turns ratio for each pair. If we designate the equivalent capacitance on the primary side as C'_N, and assume that the transformer is ideal (loss less) and has a 1:1 voltage transformation at the peak voltage V_o for the gage, then from energy considerations we can write

$$\frac{1}{2} C'_N V_o^2 = \frac{1}{2} C_o V_o^2 + \frac{1}{2} \sum_{k=1} C_k V_k^2 \tag{4.52}$$

or

$$C'_N = C_o + \sum_{k=1} C_k \left(\frac{V_k}{V_o}\right)^2 \tag{4.53}$$

Now we know the voltage on each k^{th} pair of plates (from our previous analysis) to be

$$V_k = V_o \cos \frac{2k\pi}{N} . \tag{4.54}$$

Therefore, the total measurable (transformed) capacitance of the gage is given by

$$C'_N = C_o + \sum_{k=1} C_k \cos^2 \left(\frac{2k\pi}{N}\right), \tag{4.55}$$

where C_o and C_k are obtained from (4.47) and (4.48).

Incidentally, as we mentioned in the proposal, the measured capacitance C'_N can be enhanced (if small) by adjusting the turns ratio of the transformer so that the voltage on the primary side is less than V_o.

V. EXPERIMENTAL PROGRAM

The experimental portion of the program was divided into two distinct parts. The first part consisted of a parallel work effort involved in the design and fabrication of the tank/gage hardware and the electronic circuitry. The second part involved actual experimentation with both the circuitry and the complete gaging system.

Unfortunately, the experimental work, which was designed to establish ultimate concept feasibility, was not carried to the point where conclusive evaluations of gage performance could be made. The reason for this is attributable to three fundamental causes. First, the experimental program was delayed about a month because of some difficulties which arose in the fabrication of the model tanks. Second, the program objectives were changed shortly after the experimental work was begun. Finally, the small amount of experimentation that was performed, uncovered an unexpected problem in the measurement concept, which could not be corrected in the allotted time. We will discuss this problem more fully in Section 5.5.

5.1 Model Tank Fabrication: In designing the tank hardware, it was decided to keep the model relatively small so that large volumes of test fluids, etc., would not have to be used in the test program. A dimensioned drawing of the model tank is depicted in Figure V-1. It was designed with two goals in mind; first, that in large measure, it would be a scale model of the SIVB with respect to relative dimensions (not including wall thickness); second, that it would be a design which would allow accessibility to internal surfaces during electrode installation and the test program. To meet the latter goal, the tank was designed with a flat removable top. The bottom is spun in a perfect hemispherical shape to simulate that portion of the SIVB geometry, and to allow for the investigation of electrode design in this region. The tank is constructed of .04 inch thick aluminum: sheet aluminum is used for the cylindrical portion; the end cap is spun aluminum. Two identical tanks were constructed.

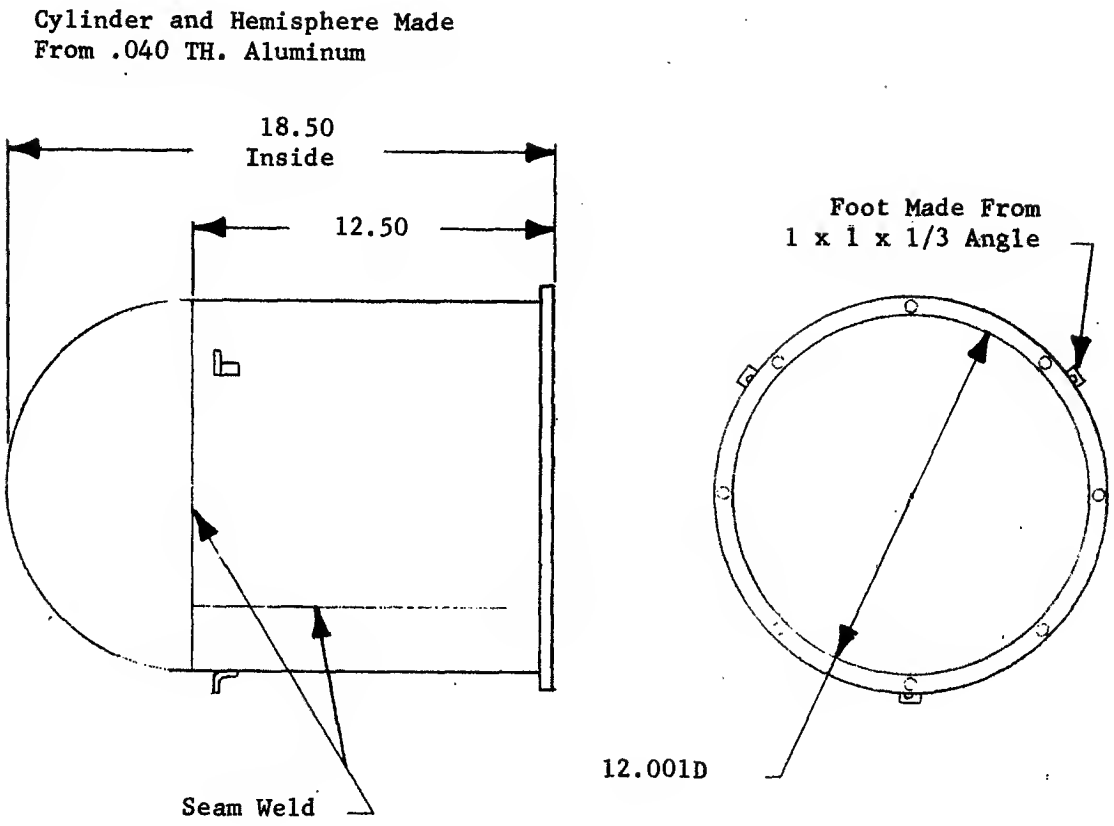

Fig.V-1 Missle Tank-Fuel Simulated

5.2 Gage Fabrication: As a result of the electrode design analysis, it was decided to fabricate the first gage using twelve electrodes. The choice is based primarily on two considerations: first, it is desirable to use a configuration from the orthogonal symmetry group N = 4, 8 12...) so that averaging could be utilized eventually; second, the case of N = 12 is one in which the resultant field is highly uniform over 80% of the tank volume, but still possesses some non-uniformity which can be studied. Furthermore, it was desirable to keep the number of electrodes as small as possible to ease the cabling problem and keep the electronics simpler.

The electrode configuration was not designed so that averaging could be used. Thus, instead of installing patch sensors in the hemispherical portion of the tank, the strips were extended continuously from one side of the tank to the other, through this region, each following the proper unidirectional field potential.

The electrode fabrication required two attempts before a successful unit resulted. In the first attempt, the gage was designed as a separate unit so that it could be removed from tank in the advent of a needed replacement. This required constructing the electrode array on a wooden mandrel as shown in Figure V-2. The twelve electrodes were fabricated from copper screen of small mesh. The screening was held in place with tape on the mandrel and then coated with an epoxy resin. To prevent the epoxy from adhering to the wooden mandrel, the latter was impregnated with a sealant, waxed and coated with a thin layer of teflon.

After the resin had cured, the outside of the electrode structure was machined to conform to the inside walls of the tank. At this point, a major problem arose. During the curing of the epoxy, some of the copper screening lifted away from the mandrel. This meant that the assembly could not be turned down enough to fit the aluminum tanks without machining away the screening at these high spots. This technique was abandoned.

In the second approach, it was decided to make the gage and tank one unit. For this case, the inside surface of the tank was coated with a thin layer of epoxy to provide the insulation between the electrodes and the tank. The electrodes were fabricated directly on this layer using copper foil tape. With this construction technique, it was possible to accurately control the shape and spacing of electrodes.

As part of the preparation for the test program, a test stand was designed and constructed which serves as a gimballed supporting structure for the tank. The set of gimbals allows two degrees of rotational freedom for the tank so that testing with liquids can be made at various tank orientations. The stand is depicted in Figure V-3.

5.3 Electronics Design and Testing: The task to demonstrate feasibility of the proposed capacitance measuring scheme was divided into two portions. First, the basic measuring scheme was demonstrated using an air variable capacitor to simulate the tank but without having the tapped transformers or the multi-segment electrodes in the model tank. The second portion of the task was to include the tapped transformers and actual tank electrodes. The reason for the division was to permit careful testing of the electronic measuring circuit using the precision air variable capacitor to simulate the tank. The division also allowed parallel fabrication of the tank model to proceed. The basic measuring circuit is shown in Figure V-4 with both the actual and the equivalent tank circuits. The parameter values for the equivalent circuit are also shown in Figure V-4. They were chosen to be representative of the values to be expected from the model tank. Operating frequencies for initial tests are also noted. The functions of oscillator amplifier and demodulator were performed in the demonstration electronics by Lock-In-Amplifier is shown in Figure V-5. It can be seen that the reference channel tuned amplifier together with the amplitude

Figure V-2

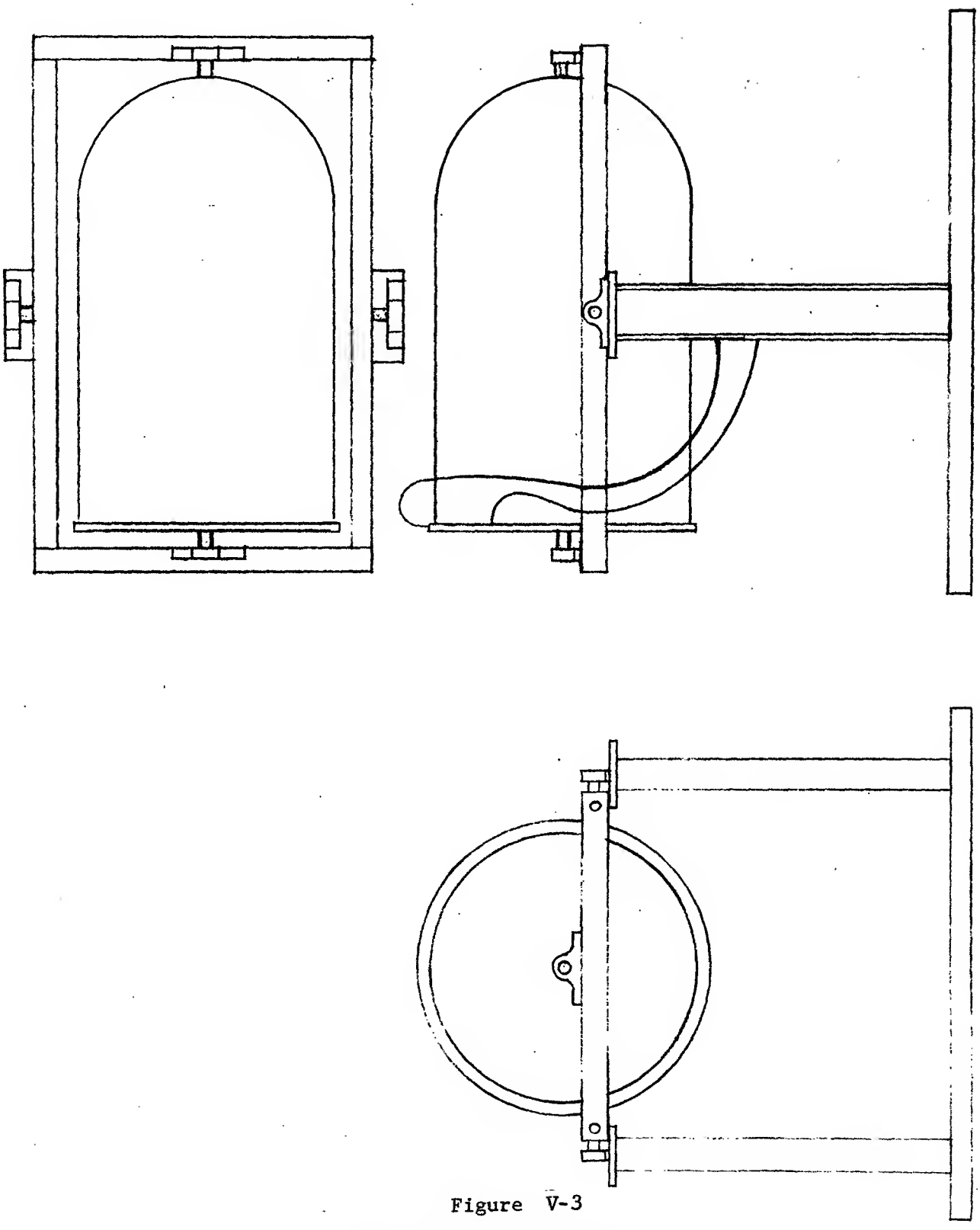

Figure V-3

Gimballed Support Stand

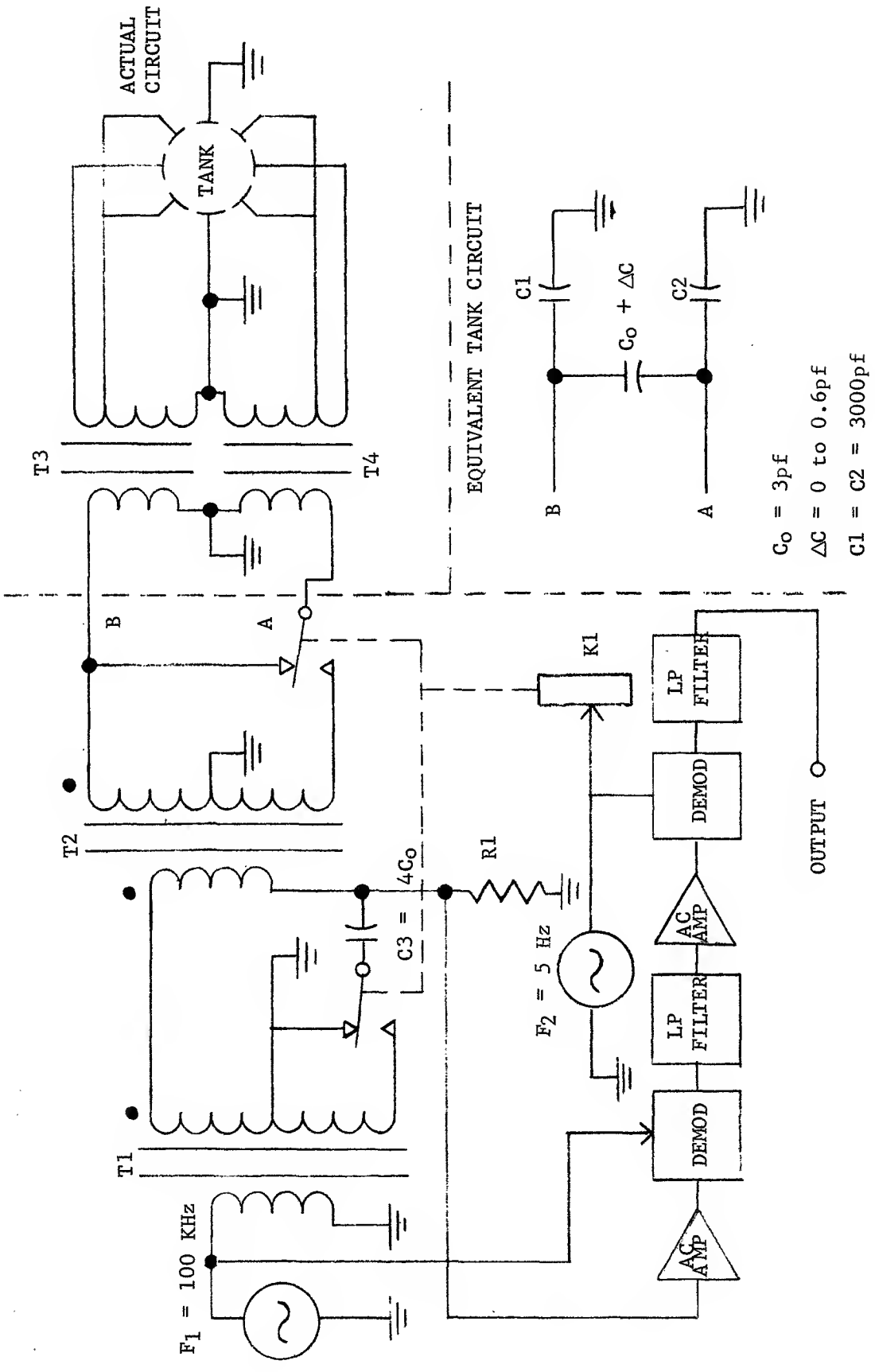

Figure V-4
CONCEPTUAL SCHEMATIC

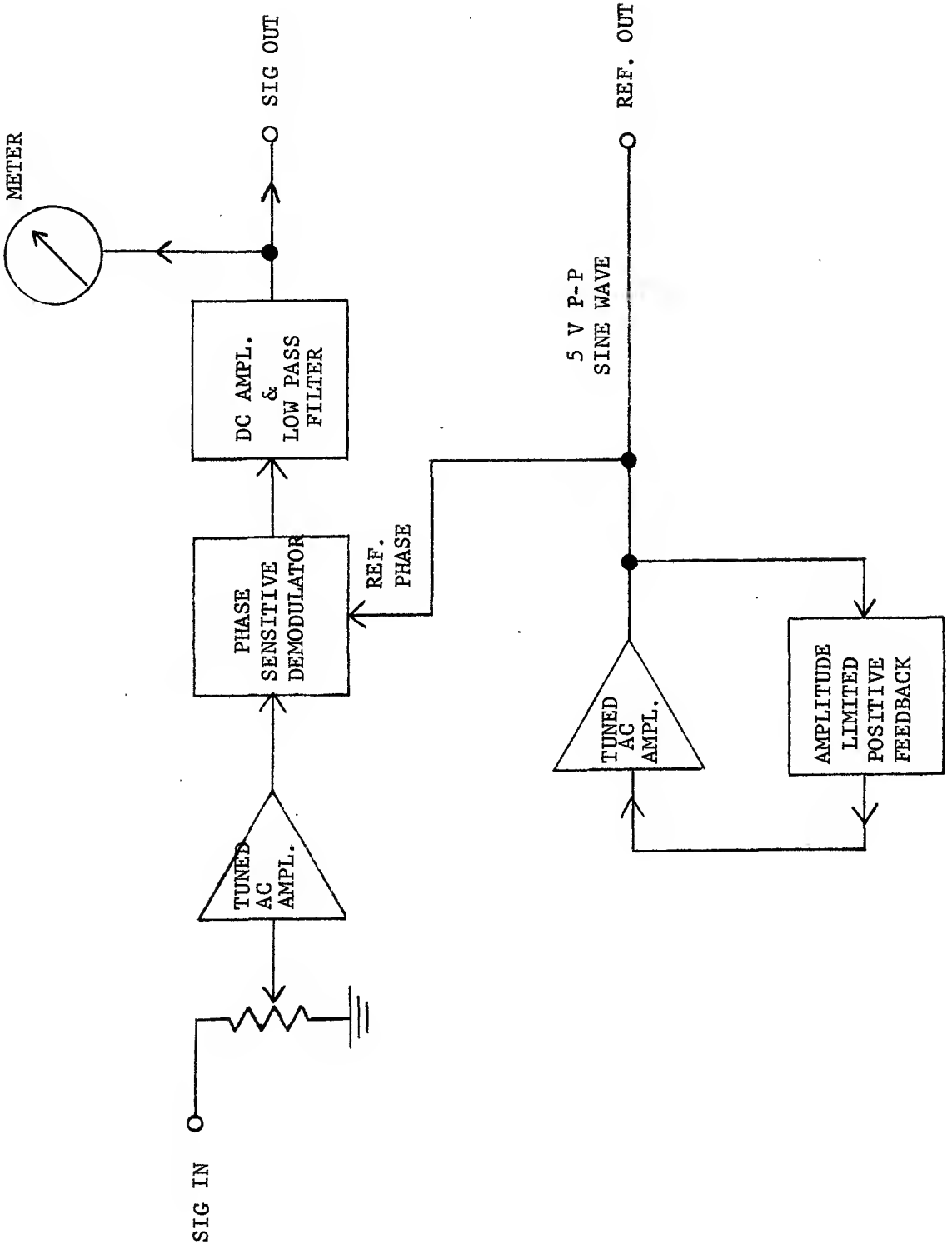

Figure V-5
BLOCK DIAGRAM JB5 LOCK-IN AMPLIFIER

limited positive feedback make an oscillator. The oscillator output is fed to the external circuitry and is used as the reference phase for the phase sensitive detector in the Lock-In-Amplifier. In the signal channel preceding the demodulator, there is a tuned amplifier which has a characteristic similar to that of a tuned circuit with Q = 25. Following the demodulator there is a low-pass filter and DC amplifier.

A specific experiment which has been performed will now be described. This experiment is the first feasibility experiment and used the circuit shown in Figure V-6. The first Lock-In-Amplifier, AR1, operates at 100 kilo-hertz and puts out five volts peak to peak from its REF OUT terminals. The voltage drop across R1, proportional to current in the primary of T1, is applied to the SIG IN terminals and has a very small amount of amplitude modulation, synchronous with the operation of relay K1. The output of AR1 is connected to the SIG IN terminals of Lock-In-Amplifier AR2 in order to recover the small modulation signal. The output of AR2, then, should be proportional to the unknown capacitor C1.

The circuit was built and tested with the values as shown in Figure V-6. These component values are those of the equivalent circuit of Figure V-4 except that the shunt capacitors C3 and C4 are 1,000 picofarads each instead of 3,000 picofarads. It was possible to obtain a full-scale output from A2 for a change in C1 of less than 0.6 picofarads as was planned. However, the output noise level was unexpectedly large (about 10% of full scale RMS). Turning off the modulation completely, by disconnecting the drive to relay K1, did not reduce the noise, but disconnecting the input from AR2 almost completely eliminated it. It was clear that the noise output of AR2 was due to noise modulation of the oscillator of AR1. A study of these noise sources was made.

The actual experimental circuit shown in Figure V-6 is a simplification of the conceptual circuit shown in Figure V-4. In Figure V-6,

relay K1 has only one pole and the vacuum balance capacitor C2 appears to the right of Transformer T1. C2 in Figure V-6 has the same purpose as C2 in Figure V-4.

Still another version of the circuit appears in Figure V-7. Here, the relay arm is grounded which would be desirable for an eventual solid-state switch. This circuit was tested and found to be much too dependent on stray capacitances between transformer windings. In the test, C2 has to be almost 90 picofarads to balance out the strays. While it is conceivable to use a guard shielded transformer for T1, our decision was to use the circuit of Figure V-6 in preference to that of Figure V-7.

The sources of noise were identified and the noise level significantly reduced in subsequent experiments. Principal sources of noise were:

1. The High Frequency Oscillator
2. The High Frequency Detector
3. Modulator Switching Transients

The Lock-In-Amplifier was found to be noisy both in its oscillator and detector functions.

The next experiment was to substitute a laboratory test oscillator as the high frequency oscillator. The oscillator used was a vacuum tube, Weir Bridge type, and was much noisier than the Lock-In-Amplifier. The laboratory test oscillator was also very microphonic.

A switching oscillator was tried next. This oscillator, using transistors as switches rather than as linear amplifiers, was successful. Its noise level was low enough so that other noise sources could be attacked. The circuit of the switching oscillator is shown in Figure V-8.

The detector portion of the Lock-In-Amplifier was also noisy; apparently mostly $\frac{1}{f}$ noise in its output dc amplifier. A simple diode detector was constructed and had much less noise.

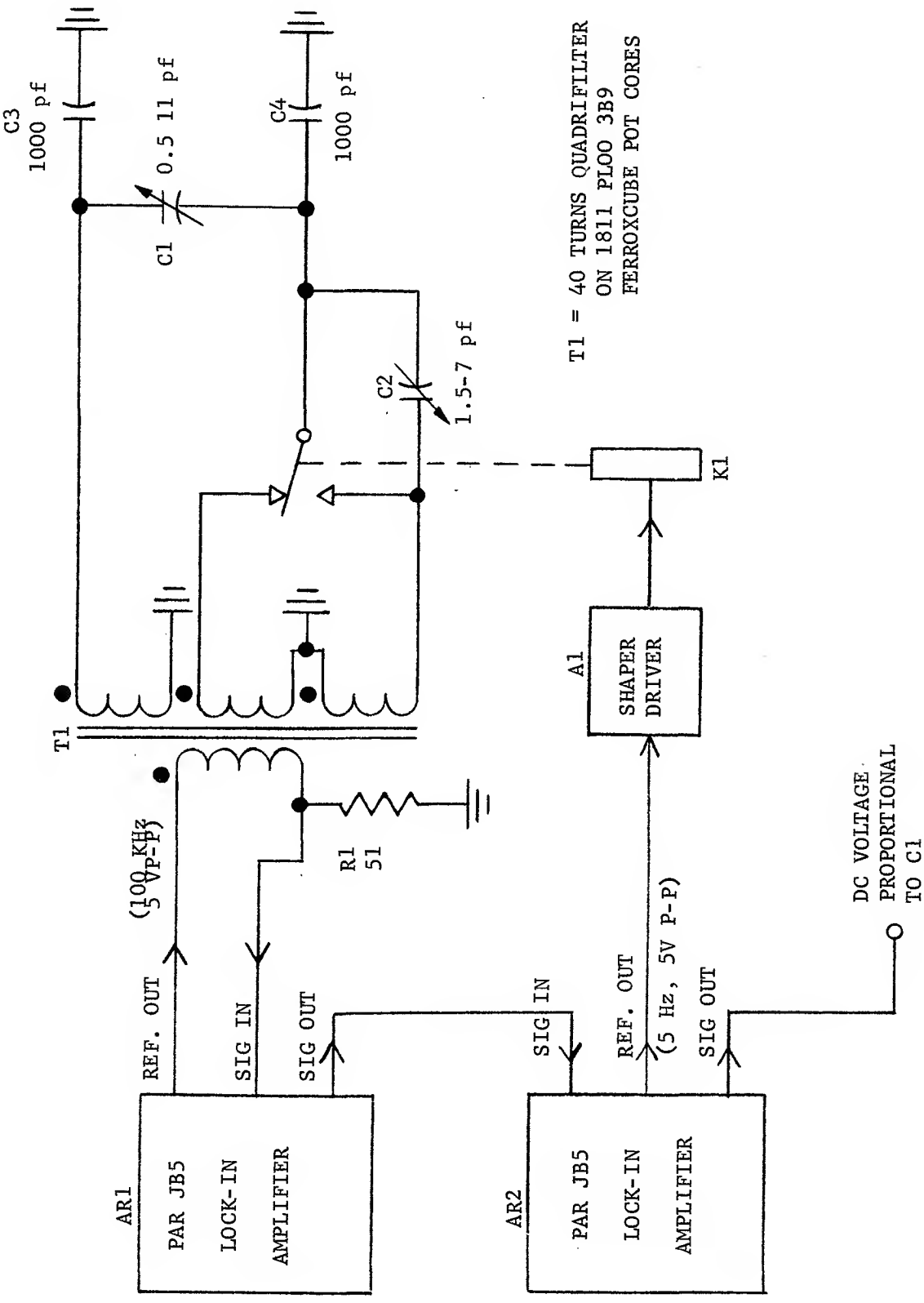

Figure V-6
EXPERIMENTAL CIRCUIT

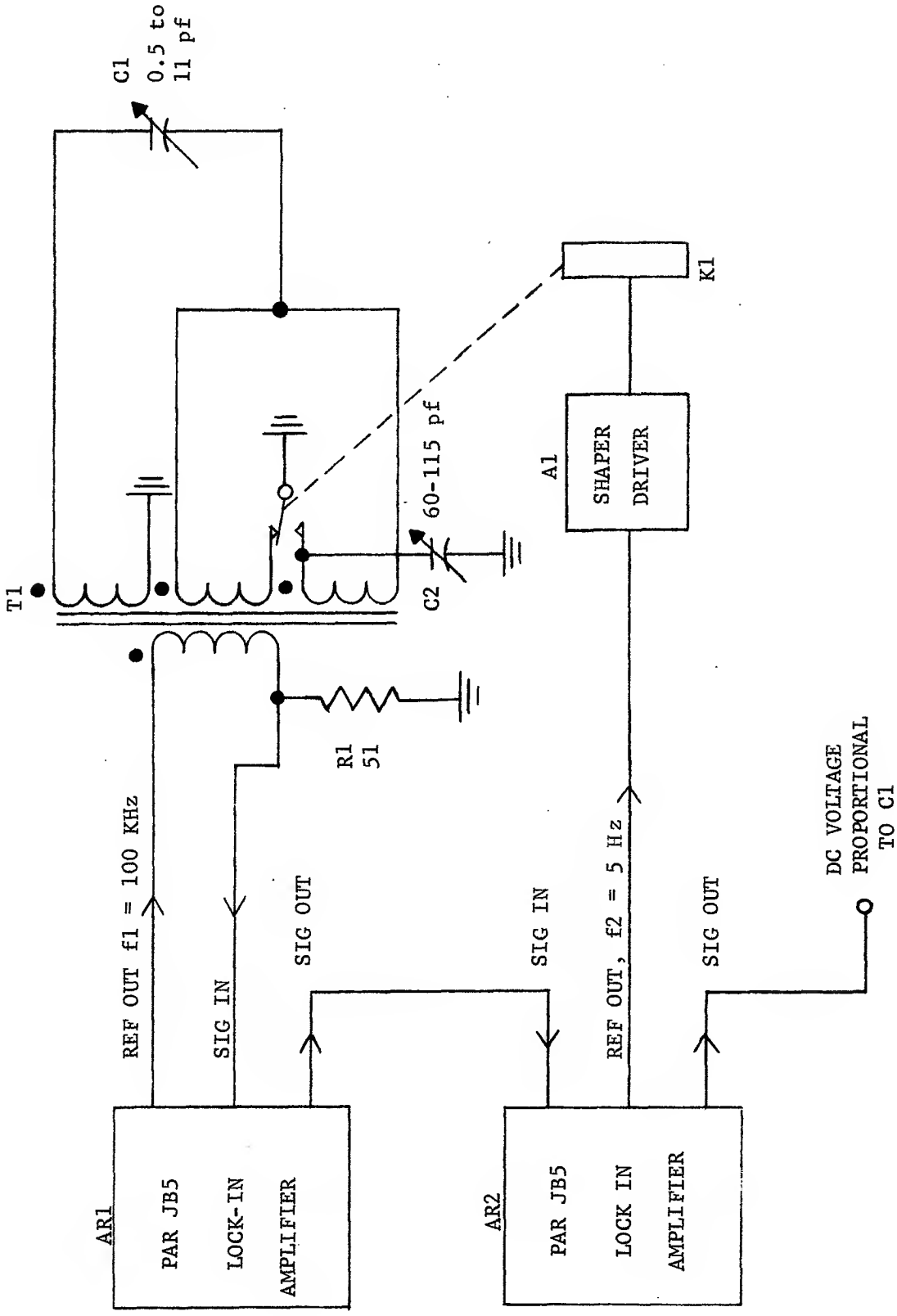

Figure V-7

UNSUCCESSFUL ALTERNATE EXPERIMENTAL CIRCUIT

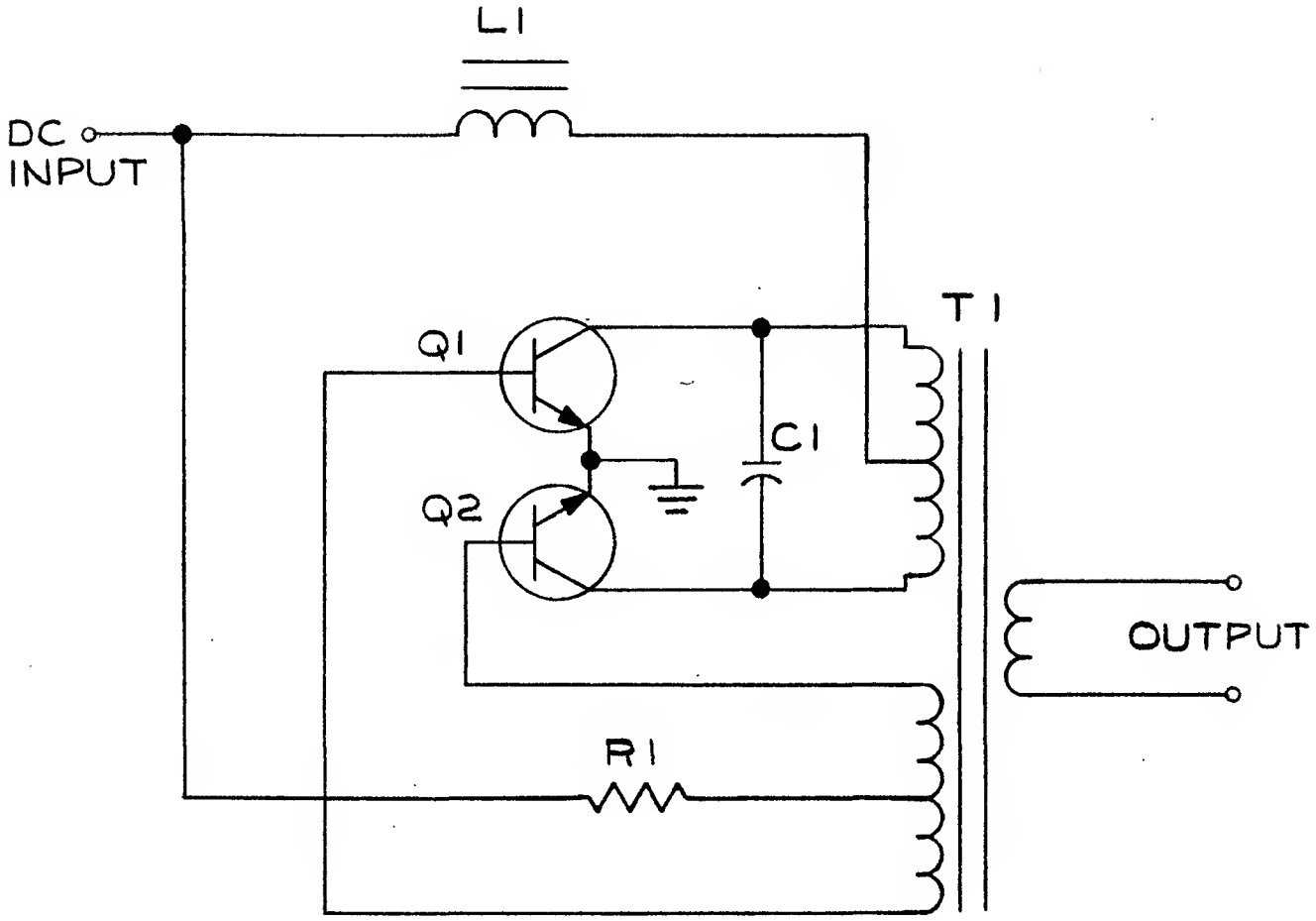

SWITCHING-TYPE SINE WAVE OSCILLATOR after BAXANDALL

FIG. V-8

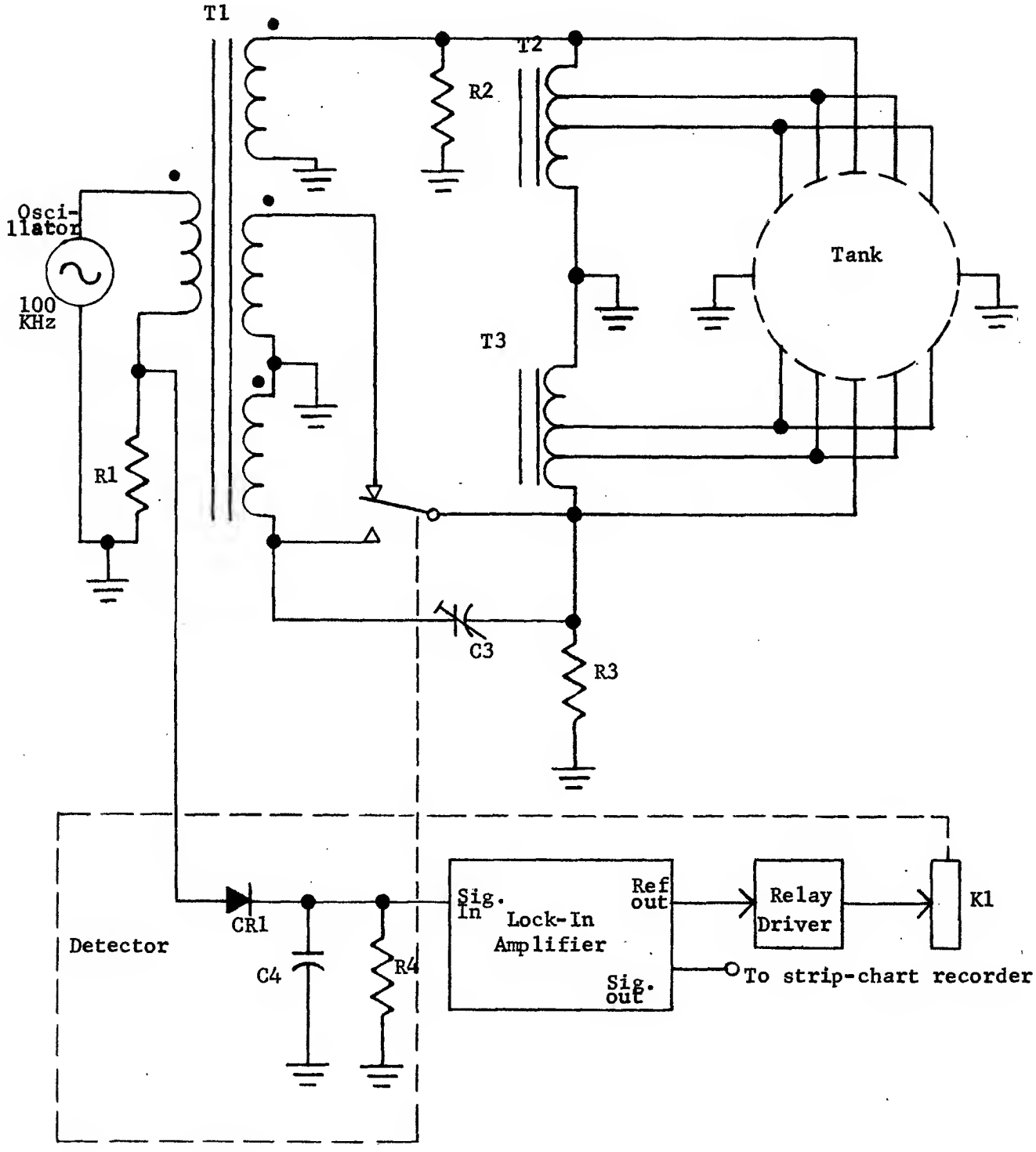

EXPERIMENTAL CIRCUIT

FIG. V-9

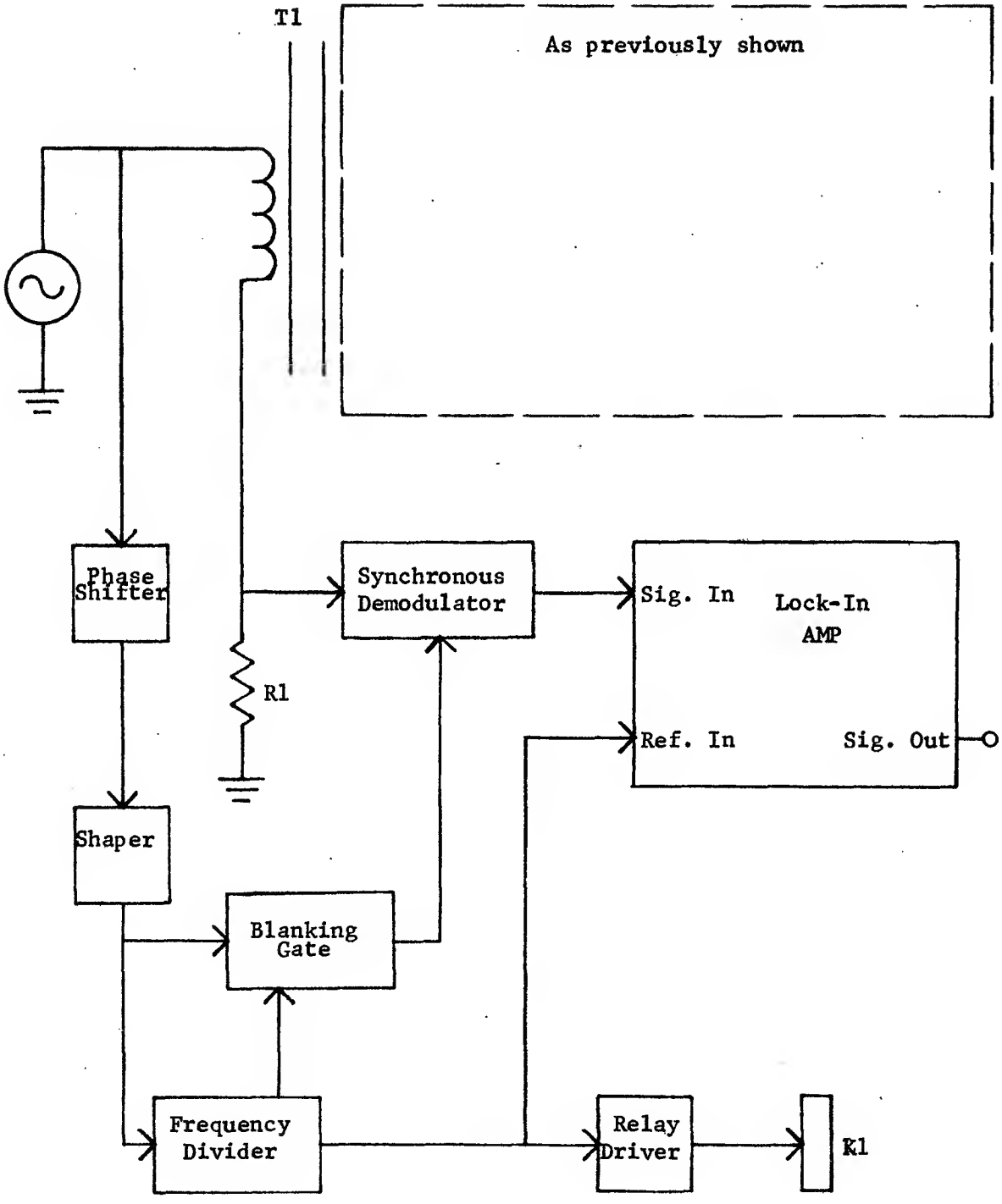

PROPOSED EXPERIMENTAL CIRCUIT

FIG. V-9b

The experimental circuit after the previously described improvements is shown in Figure V-9. A more detailed description of the circuit of Figure V-9 follows:

The oscillator is the switching oscillator (Figure V-8). T1 is a 1:1:1:1 ratio with the four windings very tightly coupled by quadrifilar winding. T2 and T3 are tapped onto transformers to give the correct electrode potentials. The taps are at 86% and 50% of the voltage. R2 and R3 are damping resistors without which the tuned circuits comprised of the transformer inductance and shunt capacitance have too high a Q. The detector is self-explanatory. The relay driver converts the sine wave at 5Hz to a square wave to drive the relay K1.

The next noise source to be attacked was that associated with modulation transients. The voltage across R1 in Figure V-9 drops to half its usual value during the "fly-time" of the relay K1 since half the shunt capacitance is disconnected then. At the instant when the contact is made, there is a transient modulation of the envelope of the voltage across R1. The magnitude of this transient depends on the phase of the high frequency oscillator at the moment of reconnection. The detector diode CR1 changes C4 to nearly the peak of the envelope, thus time spreading the transient energy.

The next modification was to use an improved detector circuit and try synchronous modulation. Figure V-9b shows the new arrangement. The synchronous modulation is obtained by dividing down the high frequency oscillator to provide the low frequency modulation. The detector circuit was changed to one with average rather than peak type response to reduce time spreading of transient peaks. Also a blanking circuit was put in the demodulator. The blanking circuit turns off the demodulator for a small fraction of the modulation period at each switching time, hence disregarding the transients.

After incorporating these modifications, the performance of the system was verified using a General Radio precision variable capacitor. The signal-to-noise ratio was found to be greatly improved so that preliminary testing of the gaging system could begin.

5.4 Gaging System Tests and Evaluation: During a visit by NASA early in December, the first gaging system test was performed in the form of a demonstration.

At this time, the modifications to the electronics had been incorporated, and the new tank had been completed except for some details of the cover; also, the fittings for filling and draining had not been added. Accordingly, the demonstration was performed without the cover.

Various amounts of RP-1 were poured into the tank. The results demonstrated a slight nonlinearity with liquid volume (approx. 4% of full-scale). The tank was tilted in various directions and amounts; some sensitivity to the orientation of the surface was observed, but the amount of variation did not seem excessive.

Fittings were later added to the tank to permit filling and draining with the cover in place.

After completing the cover and adding fittings, more data were taken with high resolution, and it was observed that the output was more nonlinear with liquid volume than had been anticipated.

Figure V-10 shows data taken with the tank axis in two different orientations. There is far more separation between the two curves than anticipated and the curves are much more nonlinear than expected. The reasons for these results have been analyzed, and the non-linearity appears to be due to three basic causes. Each cause produces a different non-linear characteristic in the response curve of Figure V-10. The three characteristics which we refer

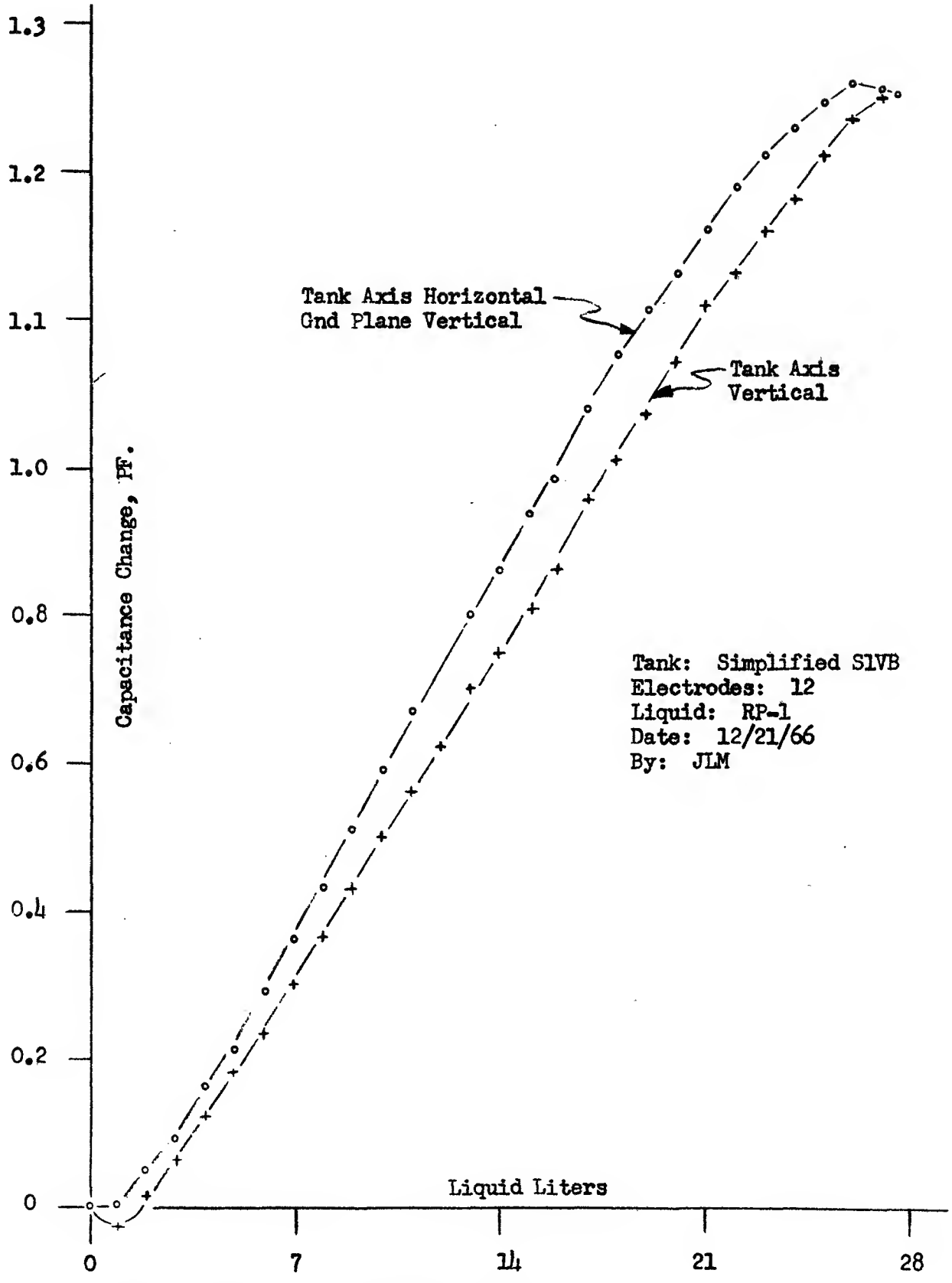

Figure V-10 Linearity Data

to here are (1) the general separation of the two curves which is greater than expected, (2) the divergence of these two curves with increasing volume of liquid and, (3) the tapering off of the response at both empty and full tank. The cause for the large separation in curves is apparently due to a fundamental problem in the measuring circuit. Because it is a concept difficulty, we will discuss this point more fully below.

The divergence of the curves appears to be attributable to the existence of the center electrode which is maintained at ground potential. Because the electrode is grounded, the fluid in the immediate vicinity of it does not get measured. When the tank is in the vertical position, more of this electrode is under fluid than when the tank is horizontal; and, therefore, less fluid is measured. This discrepancy increases until the tank is almost full. However, this difference is not large compared to the curve separation which is due to the concept problem.

The tapering off of the response curves at the full and empty points is attributable to both the ground plane effect and the highly non-uniform field near the electrodes in the end caps, especially for the flat cover. Because the unidirectional electrode configuration used in this gage is not an optimum one, the existence of these inhomogeneities is not surprising.

These two problems are solvable. The grounded electrode can be floated relative to the grounded tank wall and, thereby, be included in the measuring circuit by an additional set of leads from the transformers. The inhomogeneity problem can be corrected by shaping the electrodes in the dome.

5.5 Concept Problem: The first measurements made with a model tank and breadboard electronic unit using the principles outlined in this report yielded two unexpected results:

1. The change in capacitance when the model tank was partly filled with liquid was only about half of the expected value.

2. The nonlinearity of capacitance change with liquid volume was much greater than anticipated.

A review of the technical concepts led to the following conclusions:

1. The concept that the use of a uniform field can be used to measure liquid quantity is correct; the uniform field tends to weight all volumes equally.

2. The idea upon which the original electronic unit design is based is incorrect; the reversing of the sign of the potential on half of the tank boundary does not result in zero internal capacitance.

The scheme outlined in the proposal and implemented in the experimental program has utilized a boundary potential which has alternated between that which caused an approximately uniform field and another with the same magnitude but which resulted in no current flow across a tank diameter.

For the ideal case in a cylindrical tank, this would result in internal fields given by:

$$V_1 (r, \theta) = V_o \frac{r}{a} \sin \theta \qquad (5.1)$$

and

$$V_2(r, \theta) = \frac{2}{\pi} V_o \left[1 - \sum_{n=1}^{\infty} \frac{2}{4n^2 - 1} \left(\frac{r}{a}\right)^{2n} \cos 2n\theta \right] \qquad (5.2)$$

The purpose of this technique was to eliminate from the measurement the large capacitance from the electrodes to the tank walls. Because of the internal potential V_2 (r, θ), however, the technique also results in subtracting out part of the desired measurement. Since V_2 (r, θ) is not a uniform field, the desired equal weighting of each point in the region is not accomplished.

The electric fields represented by equations (5.1) and (5.2) are shown in Figure V-11. The capacitance of the field corresponding to V_2 is just $\frac{4}{\pi^2}$ times that of the uniform field due to V_1.

The electrodes of a uniform-field array are terminals of a multi-terminal capacitance network. More usefully, we may consider each set of electrodes which are at a single potential as a single terminal, thus reducing the complexity of the equivalent circuit. For example, consider the six electrode cylinder shown in Figure V-12. The potentials V_2 and $-V_2$ appear on pairs of electrodes.

Only four distinct potentials are used (plus ground); therefore, the equivalent network requires only five terminals including ground, as shown in Figure V-12b. Each terminal has some capacitance to every other terminal.

To prevent the figure from becoming cluttered, we have labeled only one of these capacitances in the diagram to indicate the notation to be used. Network nodes are assigned letter symbols, and the capacitance appearing between nodes is indicated by using as subscripts the symbols for the two nodes involved.

As discussed earlier, the potentials applied to the electrodes are chosen to create, within the tank, the most uniform field possible with the given electrodes. The measurement required is then the capacitance represented by this almost-uniform field. At the same time, it is necessary to insure that the measurement is not influenced by the fields between the electrodes and ground.

The capacitance which we desire to measure is readily calculated by considering the relationships in Figure V-12. The capacitances which appear directly between each terminal and ground represent fields which are outside of the electrode array; all others represent fields which are inside.

The total electrostatic energy stored on the inside of the electrode array is:

$$\mathcal{E} = 1/2 \sum_j \sum_k 1/2\ C_{jk} V_{jk}^2 \qquad j,\ k \neq G \tag{5.3}$$

The first 1/2 in this expression occurs because, due to the double sum, each capacitance is taken twice; e.g., once as C_{12} and once as C_{21}.

The capacitance we wish to measure appears across a pair of terminals which are driven with potential V_o. The energy stored in this capacitance must be the same as (5.3); i.e.,

$$\mathcal{E} = 1/2\ C_m V_o^2 \tag{5.4}$$

Therefore,

$$C_m = 1/2 \sum\sum C_{jk} \left(\frac{V_{jk}}{V_o}\right)^2 \tag{5.5}$$

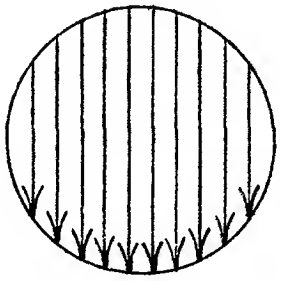

$E_1(r,\theta)$

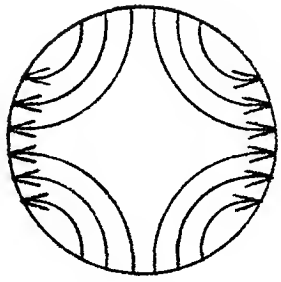

$E_2(r,\theta)$

FIGURE V-11 ELECTRIC FIELDS IN CYLINDRICAL TANK

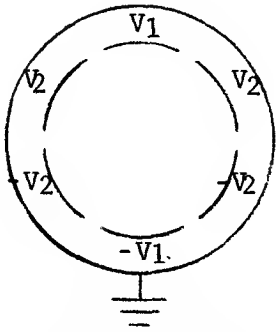

a. Electrode Array

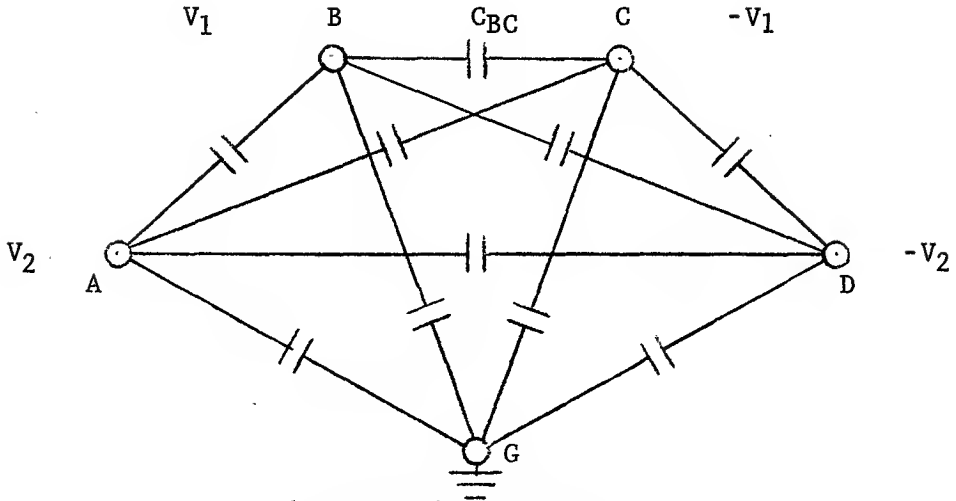

b. Equivalent Circuit

FIGURE V-12 ELECTRODES AND EQUIVALENT CIRCUIT

Equation (5.5) states that Cm may be found by measuring the C_{jk} individually and applying a weighting factor $\left(\frac{V_{jk}}{V_o}\right)^2$ to each, and adding the results; here the V_{jk} are the potentials which would be applied to obtain a uniform field. The actual value which is applied in making the measurement is, of course, immaterial.

Equation (5.5) appears to imply that both C_{12} and C_{21}, for example, are measured. Actually, of course, only one of these need be measured since $C_{ik} = C_{ki}$.

From the above discussion, it is clear that the measurement of the capacitance corresponding to the liquid quantity can be accomplished by sequential three-terminal capacitance measurements. For a system which has a large number of electrodes, this method may not result in a satisfactory system response time.

It is equally clear that other electronic systems can be devised to perform the desired measurement. For example, it is possible to devise a switching scheme which causes the electrode potentials to alternate between the cosine approximation, which yields the uniform internal field, and a set of identical potentials, which yields zero internal field. By properly weighting the currents flowing to the various electrodes, and subtracting the second set of currents from the first, it is possible to obtain a square-wave modulation which has an amplitude proportional to the desired capacitance. This scheme is capable of rapid response.

APPENDIX A

In this appendix a brief calculation is given for the required boundary potentials at the tank surfaces which give an absolutely uniform electric field E within the tank. Two ideal cases will be considered, namely an infinitely long cylinder and a sphere. An idealized representation of the actual S-IVB tank (see Fig. A1) can be obtained by cutting the cylinder for the appropriate length and fitting two hemispherical domes at each end. The bulkhead separating the LOX tank from the LH_2 tank is also assumed to be hemispherical, for convenience. This idealization results in a spherical LOX tank. The tank problem is solved by equating the potentials and electric fields along the junctions.

We consider the cylinder first. Since we assume the cylinder is of infinite length the problem is simply two dimensional; see Fig. A2. The appropriate coordinates for the problem are the polar coordinates (r, θ). It is easy to see from the figure that if the electric field E is to be everywhere constant and uniform within the circular boundary $r = R$ and in the direction indicated, then the line AA' is a ground potential ($V = 0$), by symmetry. Thus the product of the field E and the perpendicular distance from AA' to the point (r, θ) must be equal to the potential difference $V(r, \theta)$ between these points.

Therefore,

$$V(r, \theta) = E\, r \cos \theta. \qquad \text{(A-1)}$$

Similarly the potential at the boundary $r = R$ must be

$$V(R,\theta) = E\, R \cos \theta. \qquad \text{(A-2)}$$

We can arbitratily define ER = V_o, so that the potential anywhere inside r = R becomes

$$V(r, \theta) = V_o \frac{r}{R} \cos \theta, \tag{A-3}$$

and the boundary potential is dependent only on θ through the relation

$$V(\theta) = V_o \cos \theta \tag{A-4}$$

Therefore, on the cylindrical portion of the ideal tank we must apply the potential (A-4) to produce the uniform field $E = V_o/R$ everywhere inside. In the case of the LOX tank, which is assumed to be spherical for convenience, the problem is three dimensional. Again the cross-section AA' (see Fig. A3) is at ground potential by symmetry and thus the same field E times the perpendicular distance between AA' and the point (r, θ, ϕ) must be equal to $V(r, \theta, \phi)$. Thus inside the tank,

$$V(r, \theta, \phi) = V_o \frac{r}{R} \sin \phi \cos \theta, \tag{A-5}$$

and at the wall, r = R we have

$$V(R, \theta, \phi) = V_o \sin \phi \cos \theta. \tag{A-6}$$

In these relations we have defined V_o = ER, as before, so that the values of E and V at the junction of the hemisphere and cylinder are matched.

The potential distribution (A-6) completely solves the cases of the simplified geometry of the LOX tank and the domes of the hydrogen tank, while equation (A-4) solves the problem of the cylindrical LH_2 tank wall.

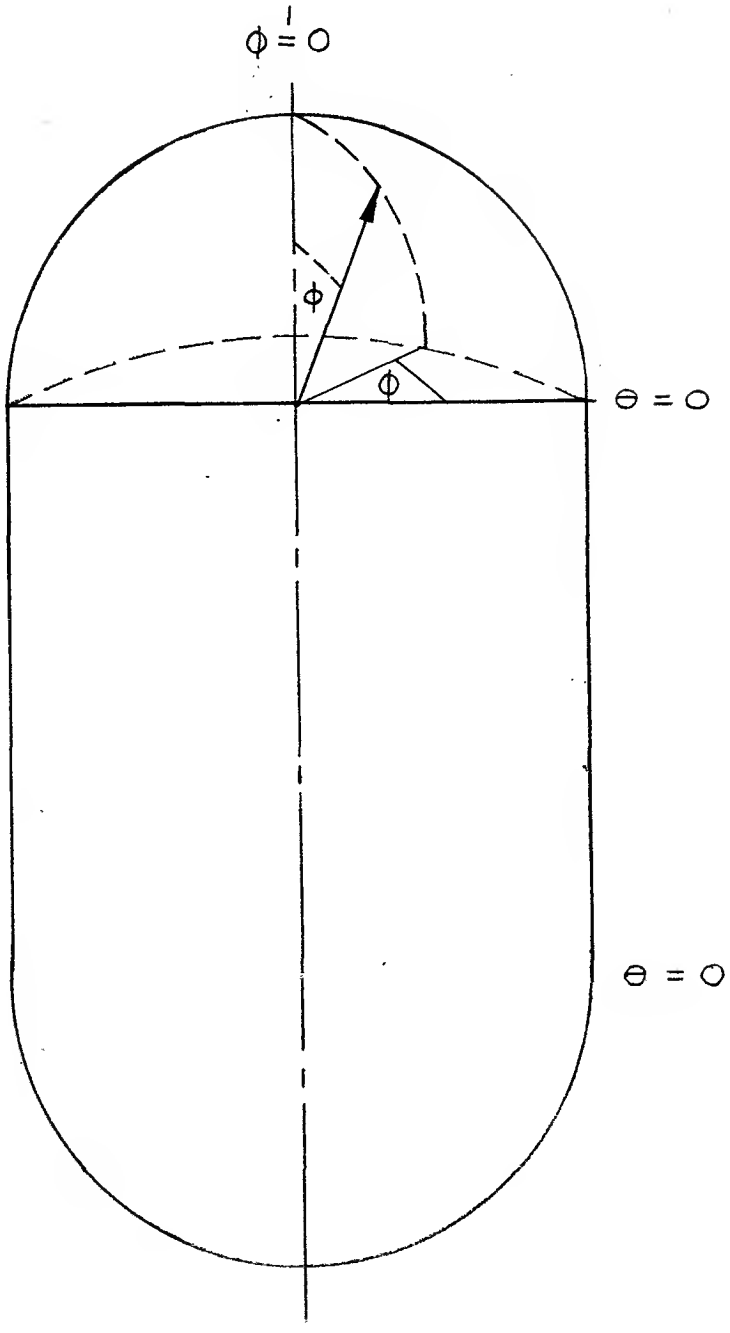

Figure (A1)

Idealized Propellant Tank

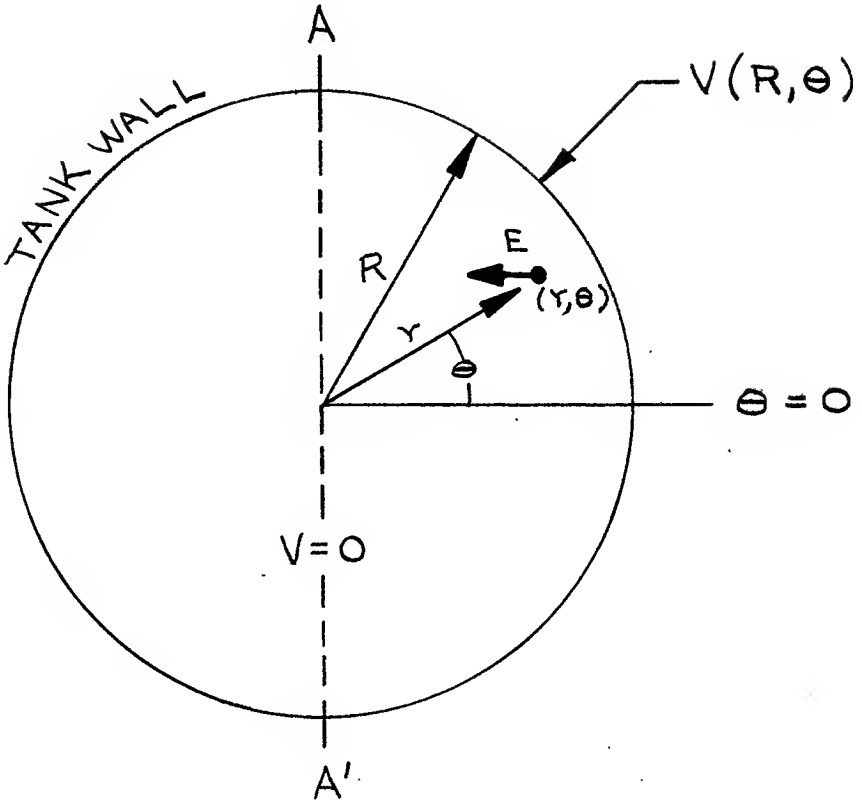

Figure (A2)
Cylindrical Geometry

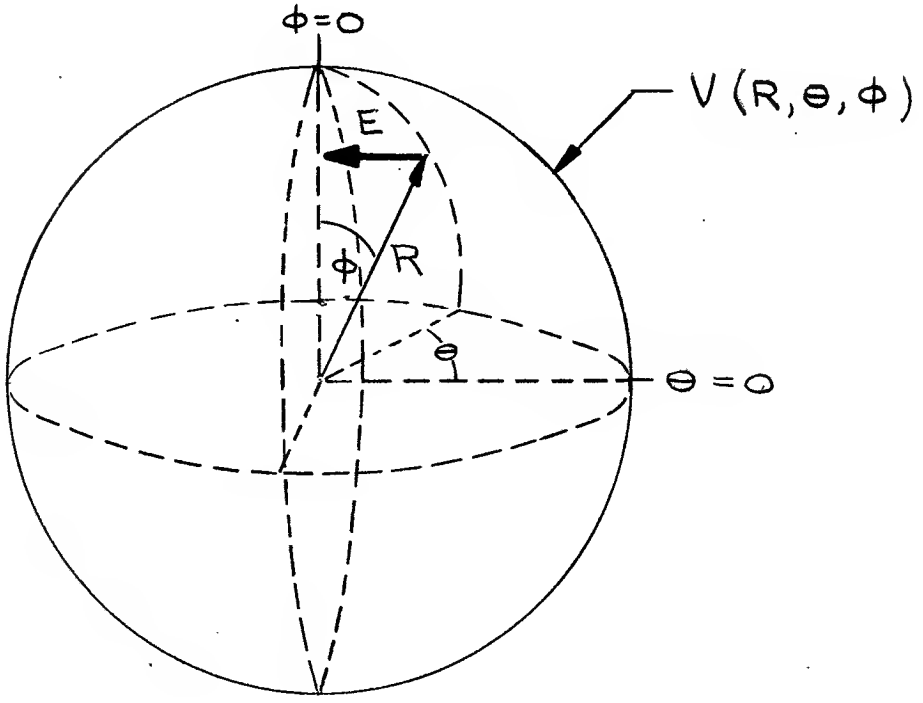

Figure (A3)
LOX Tank Geometry

APPENDIX B

The Mean Square Error Integral Function

The minimization of the Mean Square Error Integral Function is a standard mathematical technique for representing a known function in terms of a linear series expansion of orthogonal functions. To take a simple example, which is analogous to the problem in the text, let us assume that we want to represent an arbitrary function f(x), as well as possible, over an interval $a \leq x \leq b$. Furthermore, we want to represent it by a series sum of a complete set of orthonormal functions $\phi_k(x)$ defined over the same interval. Such a set might be sines and cosines or Bessel functions, etc. This is immaterial. Mathematically, we desire:

$$f(x) = \sum_k A_k \phi_k(x); \text{ over } a \leq x \leq b \tag{B-1}$$

where the A_k are constant coefficients. To represent f(x) accurately by the right hand side, we must adjust the magnitude of each of the A_k appropriately. In general, at each point x there will be some discrepancy, or error, $\epsilon(x)$ in this equality which we can represent as:

$$f(x) = \sum_k A_k \phi_k(x) + \epsilon(x)$$

or

$$\epsilon(x) = f(x) - \sum_k A_k \phi_k(x) \tag{B-2}$$

We can reinterpret f(x) as an average value of $\sum A_k \phi_k$, and the problem then becomes one of adjusting the A_k so that $\epsilon(x)$ is a very small deviation at each point. This amounts to saying that we want $\sum A_k \phi_k$ to be as close to its average value f(x) as possible. The procedure for minimizing the deviations $\epsilon(x)$ is just one step removed from just computing the statistical RMS deviation of a set of data from its average; i.e., if one has a large set of N data points X_i, with an average $\bar{x} = \frac{1}{N} \sum_i x_i$ then the average squared deviation is, by standard statistical procedure:

$$\overline{(\Delta x)^2} = \frac{\sum_i (\bar{x} - x_i)^2}{N} \tag{B-3}$$

The Mean Square Error Integral Function defined in the text is just this statement written for a continuous set of data (functions) instead of a discrete set. The correspondence is:

$$(\overline{\Delta x})^2 \longrightarrow M$$

$$\sum \longrightarrow \int_a^b \ldots dx$$

$$\bar{x} \longrightarrow f(x)$$

$$x_i \longrightarrow \sum_k A_k \phi_k(x) \qquad \left\{ \text{i.e., different "data points" for different } A_k. \right.$$

$$N \dashrightarrow \int_a^b dx$$

Written out for the continuous case using B-2, the analog becomes,

$$M = \frac{\int_a^b \left[\epsilon(x)\right]^2 dx}{\int_a^b dx} = \frac{\int_a^b \left[f(x) - \sum_k A_k \phi_k(x)\right]^2 dx}{\int_a^b dx} \qquad \text{(B-4)}$$

Now, the fitting of $\sum_k A_k \phi_k(x)$ to $f(x)$ is equivalent to minimizing M by adjusting the "data points" so that they coincide with the average; this is equivalent to a dishonest experimentalist adjusting every x_i in (B-3) so that each is equal to $\bar{x}$ (the number he wants) and, thus, the data has no experimental errors. In our case, we just adjust the A_k so that M is a minimum and we can do this by a calculus of variations technique; i.e., by computing:

$$\frac{\partial M}{\partial A_k} = 0 \qquad \text{(B-5)}$$

In the present example, if carried out using B-4, this would result in an expression for the desired A_k, which is:

$$A_k = \frac{1}{b-a} \int_a^b f(x)\phi_k(x)dx$$

Notice that if the ϕ_k were sines or cosines with the interval endpoints $b = \pi$, $a = 0$ then this expression would be the familiar Fourier coefficients relation; i.e.,

$$A_k = \frac{1}{\pi} \int_0^{\pi} f(x)\cos x \, dx$$

In terms of the uniform field problem, we are using this procedure (which is more involved computationally, but the same in principle) to find the coefficients V_k and α which allows $\phi_N(\alpha, V_K, r, \theta)$ to represent $\phi_o(r,\theta)$ as closely as possible.